Forecasting Research

Met O 11 Scientific Note No. 7

Implicit finite difference methods for modelling discontinuous atmospheric flows

by

M.J.P. Cullen

June 1988

Meteorological Office (Met O 11)
London Road, Bracknell, Berkshire RG12 2SZ, England

MET O 11 SCIENTIFIC NOTE N° 7

IMPLICIT FINITE DIFFERENCE METHODS FOR MODELLING DISCONTINUOUS ATMOSPHERIC FLOWS.

M.J.P. Cullen

LONDON, METEOROLOGICAL OFFICE.
Met.O.11 Scientific Note No.7

Implicit finite difference methods for modelling discontinuous atmospheric flows.

04911088 551.511.32 517.9 FH2A

Met O 11 (Forecasting Research)
Meteorological Office
London Road
Bracknell
Berkshire RG12 2SZ
ENGLAND

This paper was presented by Dr. Cullen at the Conference on Numerical Methods for Fluid Dynamics, 21-24 March 1988.

July 1988.

Abstract:

An important model for describing discontinuous atmospheric flows is obtained by making the geostrophic momentum approximation. The solutions vary smoothly along trajectories but may be discontinuous in an Eulerian sense. An implicit finite difference method is presented for modelling such flows. It is demonstrated that it is able to approximate the correct solution in two test problems.

1. INTRODUCTION

It is well known that finite difference and related methods will converge to smooth solutions of differential equations if they are consistent and stable. If the desired solutions are discontinuous, they are not strictly solutions of the differential equations as given, but may be solutions of a 'weak' form of the equations. Such solutions may not be unique unless extra constraints are given, such as the entropy condition for shocks in compressible gas dynamics. Finite difference schemes are not guaranteed to converge to such solutions unless they are consistent with the weak form of the equations and satisfy the extra constraints.

In meteorology an important type of discontinuous solution is a contact discontinuity whose geometry is determined by the requirements of balance between the horizontal pressure gradient and the Coriolis acceleration resulting from the earth's rotation. Such solutions can be obtained by making the geostrophic momentum approximation in the equations of motion. This is one of a number of standard approximations used in meteorology, see [1] for a recent discussion. It was introduced by Eliassen, [2] and Hoskins [3]. Smooth solutions of the resulting equations can be obtained analytically in a number of cases by using the geostrophic coordinate transformation, Blumen [14]. This linearises the evolution equations and transfers the nonlinearity to the transformation back to real space. Hoskins and Bretherton [10] demonstrated the formation of discontinuities from smooth initial data by this method. However, the geostrophic coordinate transformation becomes multivalued, and hence gives an unphysical solution, after the initial formation of a discontinuity. A method of continuing the solution after the formation of a discontinuity which makes physical sense was introduced by Cullen and Purser [4]. This continuation respects the Lagrangian form of the original equations, which contain no derivatives except those implied by the D/Dt operator. While the properties of fluid parcels have to vary smoothly in time, the solutions do not have to be continuous in

physical space, and parcel positions do not have to vary continuously in time. The existence and uniqueness of such solutions was proved in [4] for all finite dimensional versions of the problem, subject to an extra stability condition. In a wide class of two-dimensional problems, this method gives exact solutions for piecewise constant initial data. These solutions play the role of solutions of the Riemann problem for one-dimensional hyperbolic conservation laws and can be used to provide reference solutions.

The extension of the existence proof to the infinite dimensional case by taking progressively finer approximations to the data follows from the work of Pogorelov [8], though rigorous conditions for uniqueness have not yet been established. There is considerable observational support for the physical usefulness of such solutions, [5], [6].

For practical use of such a model, it is desirable to be able to approximate these solutions by conventional Eulerian finite difference schemes because no Lagrangian technique is yet available which could deal effectively with the full three-dimensional atmospheric problem. It is not clear whether an Eulerian method can approximate such solutions, because the Eulerian form of the equations will not have classical solutions once discontinuities have developed. It has not yet been established whether the Lagrangian solution of Cullen and Purser corresponds to a weak form of the Eulerian equations, or to the inviscid limit of the Eulerian equations with viscosity added. In this paper we attempt to answer this question empirically, by attempting to solve two-dimensional problems where the Lagrangian solution is exact with standard finite difference techniques. The Lagrangian solutions are calculated by an algorithm developed by Chynoweth, [7], from the existence proof in [4]. It was shown by Cullen [15] that it gives the same solution as would be obtained by the geostrophic coordinate transformation in cases where both can be used.

2. MATHEMATICAL MODEL

This section summarises the equations and the construction of Lagrangian solutions to the extent needed to choose appropriate finite difference approximations. The meteorological justification is given in [4] - [6], and the proofs are set out in full in [4] and [8].

The equations are written in a terrain-following vertical coordinate σ which is pressure p divided by surface pressure p_*. They are written in terms of the geostrophic wind defined by

$$f u_g = - \frac{\partial \phi}{\partial y} - RT \frac{\partial \ln(p_*)}{\partial y} , \quad f v_g = \frac{\partial \phi}{\partial x} + RT \frac{\partial \ln(p_*)}{\partial x} \qquad (2.1)$$

where ϕ is the geopotential whose horizontal derivative is the pressure gradient force, and f is the Coriolis parameter. u_g and v_g are the cartesian components of the geostrophic wind. R is the gas constant and T the temperature. The atmosphere is assumed to be hydrostatic, so that

$$- \frac{RT}{\sigma} = \frac{\partial \phi}{\partial \sigma} \qquad (2.2)$$

The evolution equations are given by replacing the momentum in the equation of motion by its geostrophic value, while leaving the trajectory unapproximated:

$$\frac{Du_g}{Dt} + f(v_g - v) = 0 \qquad (2.3)$$

$$\frac{Dv_g}{Dt} - f(u_g - u) = 0 \qquad (2.4)$$

$$\frac{D\theta}{Dt} = 0 \qquad (2.5)$$

$$\frac{DV}{Dt} = 0 \qquad (2.6)$$

θ is the potential temperature, given by $\theta = T(p_o/p)^{\kappa}$ where p_o is a reference pressure, $\kappa = R/C_p$ and C_p is the specific heat of air at constant pressure. V is the specific volume of the fluid. The equations are to be solved in a region Ω with boundary $\partial\Omega$, subject to the boundary condition

$$\underline{u}.\underline{n} = 0 \quad \text{on} \quad \partial\Omega. \tag{2.7}$$

It is also possible to use periodic boundary conditions. For different applications, source terms can be specified on the right hand side of (2.3) to (2.6) and non zero velocities and fluxes of u_s, v_s and θ specified on $\partial\Omega$.

This set of equations determines the actual velocity (u,v,w) implicitly, and hence the trajectory. The direct proof, [4], that this can be done requires two further simplifications. The problem has to be solved between two fixed values of pressure, so that the boundary condition at the earth's surface is applied at a typical value of surface pressure. This device allows the equations for air motion to be written in the same form as those for an incompressible fluid. A form of Boussinesq approximation is then made, [2], which allows (2.2) to be written as

$$\frac{g\theta}{\theta_o} = \frac{\partial\phi}{\partial z} \tag{2.8}$$

and (2.6) to be written as

$$\frac{\partial u}{\partial x} + \frac{\partial v}{\partial y} + \frac{\partial w}{\partial z} = 0 \tag{2.9}$$

where $z = z(\sigma)$ is the new vertical coordinate and θ_o is a reference value of θ. The Coriolis parameter f has to be treated as constant, though it is in reality a slowly varying function of position. It appears likely that the proof can be extended to remove the need for these simplifications.

The proof rests on rewriting (2.3), (2.4) as

$$\frac{D(fy-u_g)}{Dt} = fv_g \qquad (2.10)$$

$$\frac{D(v_g+fx)}{Dt} = fu_g \qquad (2.11)$$

For convenience write $(M,N)=(v_g + fx,\ fy - u_g)$. Then the equations (2.5), (2.10) and (2.11) are Lagrangian evolution equations for M,N and θ. The constraints (2.1), (2.8) can be written as

$$(fM,\ fN,\ g\theta/\theta_o) = \nabla P \qquad (2.12)$$

where $P = \phi + \frac{1}{2}f^2(x^2+y^2)$.

The proof is made by approximating the data by piecewise constants and solving exactly. The solutions are then proved to converge to a solution for general data, as the piecewise constant approximation is refined. The approach is similar to that used by Glimm [16] to prove the existence of solutions to one-dimensional hyperbolic conservation laws by approximating the data by piecewise constants and solving a sequence of Riemann problems. In our problem, much stronger results can be obtained because of the convenient nature of the equations. The finite dimensional construction was established in [4]. This is based on the same geometrical ideas as are used to construct generalised solutions to the Monge-Ampere equation. The theory of the latter equation can then be used to prove convergence to a solution for general data, Pogorelov [8]. In order to provide as rigorous a test of the finite difference method as possible, we choose test problems where the solution can be calculated exactly for all time using piecewise constant data. Since the finite difference method will treat the initial data as smooth, it is necessary to use as high a resolution as possible in defining the data for the finite dimensional construction, otherwise there could be significant differences in the solutions resulting purely from initial data.

The solutions are constructed as follows:

(i) Divide the fluid in Ω into finite parcels with volumes V_i.

(ii) Represent the data M,N and θ as constant on each parcel at an initial time t.

(iii) Arrange the parcels within Ω to satisfy (2.1) and (2,2) by constructing a convex polyhedral approximation to the hypersurface P(x,y,z), with the volumes of the faces being V_i and with $\nabla P = (M_i, N_i, \theta_i)$ on the ith face. The existence and uniqueness of this construction is proved in [4]. The requirement that P be convex is the extra information that has to be specified to get a unique solution.

(iv) Solve (2.10) and (2,11) for new values of M_i and N_i at a time $t+\Delta t$. In the test problems used in this paper these equations can be solved analytically. In general the right hand sides of these equations will be discontinuous linear functions of (x,y,z) and must be mapped into piecewise constants. This mapping restricts the overall approximation to first order accuracy.

(v) Repeat step (iii), and continue for as long as desired.

The procedure can be extended to cases where additional terms independent of $\underline{u}$ are present on the right hand sides of (2.5), (2.6), (2.10) and (2.11). If the right hand sides depend on $\underline{u}$, it may still be possible to obtain solutions by iteration. In particular the assumption that f is constant can be relaxed. The velocity field $\underline{u}$ never appears explicitly, but can be deduced from the movement of fluid parcels.

This procedure can be used in principle to construct solutions of the equations [4], and an implementation is described by Chynoweth [7]. However, it is very expensive computationally and the first order accuracy is not adequate except for cases where the approximation in steps (iv) can be avoided by solving the evolution equation analytically. The solutions may be discontinuous in physical space and it is also possible for parcel positions to change discontinuously in time. In the latter case the velocity field $\underline{u}$ cannot be defined.

When solving the equations by finite difference methods it is necessary to ensure convergence to the limit solution described above even when it is singular. It is not yet possible to prove such convergence, and in particular it is not known what if any finite difference formulae are consistent with the equations if the solutions are discontinuous. Certain principles can be stated, however.

(i) The trajectory has to be diagnosed from the system of equations, an implicit finite difference method must be used to do this.

(ii) The consistency conditions (2.1) and (2,2) must be satisfied by volume preserving rearrangements of θ, M and N. Ideally no new values of these quantities should be created by the finite difference scheme and the volume of fluid with values of M, N and θ within a given range should be conserved. This rearrangement condition is the same as should be applied to the vorticity when solving the equations for two-dimensional incompressible flow. It favours the use of quadratically conserving centered differences of the type introduced by Arakawa [9] to mimic that constraint. If iterative methods are used to obtain solutions satisfying (2.1) and (2.2), each iteration must also consist of a rearrangement.

The boundary conditions state that it is known which fluid parcels lie in Ω at any time. However, no parcel positions are known. Fluid initially in contact with the boundary can separate from it. Though the normal velocity is zero at the boundary it can be discontinuous and non zero flow can occur arbitrarily close to the boundary. These conditions are difficult to treat correctly in a finite difference calculation.

In this paper we solve two dimensional test problems derived from equations (2.1) to (2.7). The first test problem was introduced by Hoskins and Bretherton, [10], as a model for the formulation of fronts in the atmosphere. The fronts are formed by the action of a deformation field $\underline{u}=(-\alpha x,\alpha y,0)$ on a basic horizontal

temperature gradient. The equations for the evolution of the cross-section along y=0 can be written:

$$fv_g = \frac{\partial \phi}{\partial x} + RT\frac{\partial}{\partial x}\ln(p_*) \tag{2.13}$$

$$-\frac{RT}{\sigma} = \frac{\partial \phi}{\partial \sigma} \tag{2.14}$$

$$\frac{Dv_g}{Dt} + fu = -\alpha(v_g + fx) \tag{2.15}$$

$$\frac{D\theta}{Dt} = 0 \tag{2.16}$$

$$\frac{DV}{Dt} = -\alpha V \tag{2.17}$$

$$u = \mp \alpha x \quad \text{at} \quad x = \pm \alpha L \tag{2.18}$$

$$\dot{\sigma} = 0 \quad \text{at} \quad \sigma = 0,\ 1 \tag{2.19}$$

$$\phi = 0 \quad \text{at} \quad \sigma = 1 \tag{2.20}$$

$\dot{\sigma}$ is the vertical motion relative to the coordinate σ

For Eulerian calculations write

$$\frac{D}{Dt} \equiv \frac{\partial}{\partial t} + u\frac{\partial}{\partial x} + \dot{\sigma}\frac{\partial}{\partial \sigma} \tag{2.21}$$

and write (2.17) as

$$\frac{\partial p_*}{\partial t} + \frac{\partial}{\partial x}(p_* u) + \frac{\partial}{\partial \sigma}(p_* \dot{\sigma}) = -\alpha p_* \tag{2.22}$$

where p_* is the surface pressure.

Since equations (2.13) can be written in terms of $M = v_g + fx$ as

$$\frac{DM}{} = -\alpha M \tag{2.23}$$

Dt

which can be solved analytically, the solution can be determined exactly for all time for piecewise constant initial data.

The second problem is one of flow over a two-dimensional mountain ridge. The equations are similar to (2.13) to (2.20) except that (2.15), (2.17), (2.18) and (2.20) become

$$\frac{D}{Dt}(v_g + fx) = fU. \tag{2.24}$$

$$\frac{DV}{Dt} = 0 \tag{2.25}$$

$$u = U \quad \text{at} \quad x = \pm L \tag{2.26}$$

$$\theta = \theta_o(\sigma), \quad M = M_o(\sigma) \quad \text{at } x = -L \tag{2.27}$$

$$\phi = \phi_*(x) \quad \text{at} \quad \sigma = 1 \tag{2.28}$$

This problem can also be solved exactly for piecewise constant initial data if the boundary conditions (2.26 - 2.28) are replaced by moving the mountain at speed -U through a fixed domain and not allowing any flow through the boundaries. The right hand side of (2.24) has then to be set to zero.

3. FINITE DIFFERENCE ALGORITHMS

The main purpose here is to find a stable and robust algorithm which is able to approximate these discontinuous solutions. A standard second order accurate centered scheme is used, modified as necessary to allow it to treat these cases. Further work is needed to see if upwind or higher order accurate methods would be applicable. It would be natural, for instance, to use compact differences, Beam and Warming [11].

The basic method is to use a predictor-corrector algorithm in which the fields are first updated using the velocity field from the previous timestep, and a correction to the velocity field is then diagnosed to ensure that p_*, v_g and θ satisfy the diagnostic relations at the new time-level. The structure of the solution is thus similar to a Navier-Stokes solver, where the pressure has to be corrected so that the velocity field is non-divergent at the new time-level. In order to treat non-smooth solutions it is found necessary to under-relax the corrections. In the mountain problem, fluid can 'jump' discontinuously across the ridge. This cannot be represented by advection by a velocity field and must be treated by explicit adjustment of the v_g and θ fields. Physically, the rapid transient motion in such regions cannot be described under the geostrophic momentum approximation.

Several of the considerations that arise in the choice of finite difference approximation also arise in Navier-Stokes solvers. The equation to be solved for the velocity correction takes the form of an elliptic equation for a stream-function. The discretisations is chosen to give a 5-point stencil for this elliptic equation, to avoid checkerboard instabilities. The finite difference approximations used in the predictor step have to be chosen to be consistent with those in the corrector step to ensure rapid convergence.

Though no artificial viscosity is required on physical grounds, some steps have to be taken to control numerical errors. In particular, it is found necessary to smooth the velocity field calculated at one time-step before using it as a first guess for the next time-step.

The standard difference notation

$$\delta_x A = \Delta x^{-1}(A_{x+\frac{1}{2}} - A_{x-\frac{1}{2}}) \tag{3.1}$$

$$\bar{A}^x = \tfrac{1}{2}(A_{x+\frac{1}{2}} + A_{x-\frac{1}{2}})$$

is used. The finite difference approximations to (2.13), (2.14) and (2.22) are :

$$f v_{\sigma *} = \delta_x \phi_* + RT_* \, \delta_x \ln(p_*) \tag{3.2}$$

$$f \delta_\sigma v_\sigma = -\frac{\underline{R}}{\sigma} \delta_x T + R \delta_{\geq \sigma} \bar{T}^x \, \delta_x \ln(p_*) \tag{3.3}$$

$$\frac{\partial p_*}{\partial t} + \delta_x(p_* u) + \delta_\sigma(p_* \dot{\sigma}) = -\alpha p_* \tag{3.4}$$

The suffixes * refer to values at the earth's surface, σ=1. In order to use these convenient approximations, the variables must be arranged on the grid as shown in Fig. 1. If the dimensions of the grid are M x N in the x and σ directions, equation (3.4) is applied at (M-2) x (N-2) points , u is specified at 2N boundary points and w at 2M boundary points. The vertical average of (3.4) gives, using (2.19),

$$\frac{\partial p_*}{\partial t} + \delta_x(p_*)\bar{u} = -\alpha p_*, \tag{3.5}$$

where $\bar{u}$ is the vertical mean of u.

Subtracting (3.5) from (3.4) gives

$$\delta_x(p_*(u-\bar{u})) + \delta_\sigma(p_* \dot{\sigma}) = 0 \tag{3.6}$$

This implies that there is a stream function ψ defined at (M-2)x(N-2) interior points and specified as zero at 2M+2N-4 boundary points, where

$$\delta_x \psi = p_* \dot{\sigma} \tag{3.7}$$

$$\delta_\sigma \psi = -p_* (u-\bar{u})$$

Condition (3.3) is applied at (M-1)x(N-2) points. The evolution equation (3.5) is solved at (M-1) points.

The finite difference approximations to the evolution equations (2.15) and (2.16) are

$$\frac{\partial v_\sigma}{\partial t} + u(\delta_{2x} v_\sigma + f) + \dot{\sigma}\, \delta_\sigma v_\sigma = -\alpha(v_\sigma + fx) \qquad (3.8)$$

$$\frac{\partial \theta}{\partial t} + \underline{u}^{x}_{\sigma}\, \delta_x \theta + \sigma \delta_{2\sigma} \theta = 0 \qquad (3.9)$$

The approximations to the advection terms used in these equations are chosen to be consistent with the finite difference scheme for generating the velocity correction described later.

The procedure for advancing from time t to t+Δt is a predictor corrector method suggested by that of Meek and Norbury [12]. A standard Crank-Nicholson scheme is used to step equations (3.5), (3.8) and (3.9) forward, using values of ψ and hence $(p_* u)$ and $(p_* \dot{\sigma})$ at time t. The new values of v , θ and p_* will not satisfy (3.2) and (3.3). The values of ψ are then corrected so that (3.2) and (3.3) are satisfied and new estimates made of the other quantities at time t+Δt. Each of these steps gives one or more implicit equations, each for a single dependent variable at the new time level. These are solved by a block tridiagonal algorithm as in [12] in which full inversions are done in the σ direction, and a standard tridiagonal elimination is performed on the blocks. This method is efficient for the vertical resolutions used here, but would need reconsidering at higher vertical resolutions.

The first (predictor) step can be written:

$$(v_\sigma)^* = (v_\sigma)^t + \Delta t(fU - u(\delta_{2x}v_\sigma + f) - \overline{\dot{\sigma}}^{x}_{\sigma}\,\delta_\sigma v_\sigma)^\S \qquad (3.10)$$

$$\theta^* = \theta^t - \Delta t(\overline{u^\sigma\delta_x\theta^x} + \dot{\sigma}\delta_{2\sigma}\theta)^\S \qquad (3.11)$$

$$p_*{}^* = p_*{}^t - \Delta t\delta_x(\bar{p}_*u) \qquad (3.12)$$

where superscript # denotes a provisional value at $t+\Delta t$ and § denotes the time averaging :

$$v_\sigma{}^\S = \tfrac{1}{2}(\, v_\sigma{}^t + v_\sigma{}^{t+\Delta t}\,)$$
$$\theta^\S = \tfrac{1}{2}(\, \theta^t + \theta^{t+\Delta t}\,) \qquad (3.13)$$
$$u^\S = u^t$$
$$(p_*u)^\S = (p_*u)^t$$
$$\dot{\sigma}^\S = \dot{\sigma}^t$$

The obvious method for the corrector step would be a fully coupled solution of the finite difference approximations (3.2), (3.3) and (3.10) - (3.12) using Newton's method to linearise the equations for the corrections to v_σ, θ, p_*, u and $\dot{\sigma}$. This method is successful for smooth solutions of the equations solved in this paper but fails for discontinuous solutions. The reason for the failure is discussed below. A less direct method is therefore used. A stream function correction $\Delta\psi$ is calculated from the equations :

$$\theta^\# = \theta^* - \Delta t(\,\Delta\dot{\sigma}\delta_{2\sigma}\theta^*\,) \qquad (3.14)$$

$$v_\sigma{}^\# = v_\sigma{}^* - \Delta t(\,\Delta u(\delta_{2x}v_\sigma + f)^*) \qquad (3.15)$$

$$p_*{}^\# = p_*{}^* - \Delta t(\,\delta_x\Delta(\bar{p}_*\bar{u})\,) \qquad (3.16)$$

$$\delta_x\Delta\psi = \Delta(p_*\dot{\sigma}) \qquad (3.17)$$

$$\delta_\sigma\Delta\psi = -\Delta(p_*(u-\bar{u})) \qquad (3.18)$$

$$\Delta u = \Delta(p_*u)/p_*{}^*\,,\quad \Delta\dot{\sigma} = \Delta(p_*\dot{\sigma})/p_*{}^* \qquad (3.19)$$

$$fv_{\sigma*}{}^\# = \delta_x\varphi_* + RT_*{}^*\delta_x(\ln(p_*{}^\#)) \qquad (3.20)$$

$$f\delta_\sigma v_\sigma{}^\# = -R\sigma^{-1}\delta_x T^\# + R\delta_{2\sigma}(\bar{T}^x)^*\delta_x\ln(p_*{}^\#) \qquad (3.21)$$

Equations (3.20) and (3.21) are linearisations of the exact conditions (3.2) and (3.3) to be applied at $t+\Delta t$. Equations (3.16)

to (3.18) are derived from (3.12) and (3.7) by perturbing the dependent variables. Equation (3.19) is a linearised estimate of u given p_*u. Equations (3.14) and (3.15) are obtained by perturbing (3.8) and (3.9) and selecting only certain terms. This selection is the key to a stable integration scheme. It can be understood by substituting v_σ^*, p_*^* and θ^* into (3.20) and (3.21) to obtain residuals E , and then substituting (3.14) - (3.19) into (3.20) and (3.21), giving :

$$-f\Delta t\{\ \delta_\sigma(\Delta\psi)_*(\delta_{2x}v_\sigma + f)_*^*) - \Delta t\ RT_*^*\{\delta_x\delta_x\Delta(p_*\bar{u})/p_*\} = E_* \quad (3.22)$$

$$-f\Delta t\ \delta_\sigma\{\ \delta_\sigma(\Delta\psi)_x(\delta_{2x}v_\sigma + f)^*) - \quad (3.23)$$

$$\Delta t\ R\sigma^{-1}\overline{(p/p_o)^\kappa}^{x}\ \delta_x\{\delta_x(\Delta\psi)\delta_{2\sigma}\theta^*/p_*\ \} - R\Delta t\ \delta_{2\sigma}\bar{(T)}^{x*}\{\ \delta_x\delta_x\Delta(p_*\bar{u})\ \}/p_* = E$$

Equation (3.23) contains a variable coefficient elliptic operator on $\Delta\psi$ and (3.22) contains an elliptic operator on $\Delta(p_*\bar{u})$. There are also coupling terms between the equations. The omission of the remaining terms in (3.9) from (3.14) and in (3.8) from (3.15) makes equation (3.23) more strongly elliptic than if all the terms were included. In particular all the cross-derivative terms $\delta_x\delta_\sigma$ have been removed. If these terms were retained, the equation for $\Delta\psi$ would only be elliptic if

$$(\ \partial v_\sigma/\partial x + f\ )\partial\theta/\partial\sigma - (\partial v_\sigma/\partial\sigma)\partial\theta/\partial x \geq 0 \quad (3.24)$$

while equation (3.23) is elliptic if

$$\partial v_\sigma/\partial x + f \geq 0;\ \partial\theta/\partial\sigma \geq 0; \quad (3.25)$$

a much weaker condition. The effect is to stabilise the iteration and allow it to reach discontinuous solutions of the governing equations. However more iterations are needed to satisfy (3.2) and (3.3) to a given tolerance. It is necessary to ensure that the condition (3.25) is satisfied by the data before solving (3.22) and (3.23). If necessary, the data must be modified. An appropriate method is described later. The finite difference equation (3.23) contains the five point approximation to the Laplacian operator.

If more averaging were used in the finite difference approximations to (3.14) and (3.15), which are used to generate (3.23), a nine point Laplacian would be obtained. This is well known to be susceptible to checkerboard instabilities. It is necessary to use the same approximations in (3.8) and (3.9) as in (3.14) and (3.15) to ensure effective removal of the residual E in a small number of iterations.

Equations (3.22) and (3.23) are solved for $\Delta\psi$ and $\Delta\bar{u}$ by the same block tridiagonal algorithm as used in the predictor step, and an estimate of the values of θ, v_σ and p_* at time $t+\Delta t$ is then obtained from:

$$\theta^{t+\Delta t} = \theta^{**} - \Delta t\left(\overline{\overline{\Delta u \delta_x \theta}^{\sigma}}^{x} + \dot{\Delta\sigma}\, \delta_{2\sigma}\theta \right)^{*} \tag{3.26}$$

$$v_\sigma^{t+\Delta t} = v_\sigma^{**} - \Delta t\left(\Delta u(\delta_{2x}(v_\sigma + f) + \overline{\dot{\Delta\sigma}\, \delta_\sigma v_\sigma}^{\sigma} \right)^{*} \tag{3.27}$$

$$p_*^{t+\Delta t} = p_*^{**} - \Delta t\{\Delta(p_*\bar{u})\}; \tag{3.28}$$

where § refers to an average of the intermediate value at # and that at $t+\Delta t$. The correction step is then iterated as much as necessary. The final correction (3.26)-(3.28) can be combined with the predictor step at time $t+\Delta t$.

When solving a problem with significant variations in terrain height, the simplified equations (3.14) to (3.21) are no longer sufficient to give a solution in a small number of iterations because finite differences taken along σ surfaces include vertical as well as horizontal variations. Equations (3.14) and (3.21) can be written

$$\theta^{\circ} = \theta^{**} - \Delta t\{ \delta_x(\Delta\psi)|_\sigma \delta_{2\sigma}\theta^{**} \} \tag{3.29}$$

$$f\delta_\sigma v_\sigma^{*} = -R\sigma^{-1}\delta_x T^{*}|_p \tag{3.30}$$

If the x derivative of $\Delta\psi$ in (3.29) is taken at constant p rather than constant σ it is found that a faster and more reliable convergence to the solution of the system (3.2) - (3.9) is obtained. The elliptic equation (3.23) now includes the term $\delta_x(\delta_x\Delta\psi)|_p$.

leading to a 7 point stencil for the Laplacian operator on $\Delta\psi$ as illustrated in Fig. 2.

When discontinuous solutions of the type encountered in gas dynamics are being captured by a finite difference scheme, it is necessary to include dissipation either explicitly or implicitly to give the required entropy increase. In the present model of front formation the discontinuity is a contact discontinuity and is not associated with any energy dissipation. The numerical difficulties come from the fact that conditions (3.24) and (3.25) which ensure ellipticity of the equation for the streamfunction correction cannot be enforced on the fields at the new time level and because the finite difference approximations may not be consistent at the discontinuity. The stability difficulties can largely be avoided by the use of (3.23), which usually underestimates the actual correction needed to ψ and is equivalent to the under-relaxation commonly used in the pressure correction method for the Navier-Stokes equations. The question as to whether the resulting solution is correct can only be answered at the moment by practical tests such as those given in section 4.

In the mountain flow problem, as discussed in [13], energy is dissipated when fluid jumps discontinuously from the mountain top to a new position on the lee side. In this situation the condition (3.25) is likely to be violated with $(\delta_{2x}v_g+f)$ negative at some grid points. The data have then to be modified to restore monotonicity of $v_g+ fx$ as a function of x while not changing the global mean value of v_g . It is desirable to do this in a way which is consistent with (3.2) and (3.3). This is done by modifying the potential function defined by

$$P(x) = \int^{x}_{o} (v_g + fx')\, dx' \qquad (3.31)$$

so that it satisfies $d^2P/dx^2 \geq 0$, and then calculating new v_g values from the modified function. This procedure corresponds to the discontinuous jump of fluid. Care is needed in interpreting the values of u and $\dot{\sigma}$ when this correction has to be invoked since they no longer represent the total fluid velocity.

It is natural to use the final values of u and $\dot{\sigma}$ at one timestep as the first guess for the values in the next predictor step. In practice, it is found necessary to smooth them between timesteps so that the small scale detail calculated at time t is not used in the first guess for the next timestep.

4. RESULTS

4.1 Front formation

The governing equations are (2.13) - (2.23). The domain is compressed laterally with the deformation rate α. The initial data used is shown in Fig. 3. It is similar to that used in [4] except for the choice of the basic state vertical gradient of θ. Fronts tend to form initially at the upper and lower boundaries and penetrate into the interior of the fluid. This penetration is clearly seen in the Lagrangian model by comparing Figs. 3(a) and 4(a). The solutions using the Lagrangian method described in [7] are shown in Fig. 4 after a non-dimensional time $t = 0.5$ when the domain has shrunk by a factor of approximately 0.6. Since θ is conserved following parcels, by (2.16), and M changes according to (2.23); the constraints (2.13), (2.14) require the slope of the isentropes to become shallower with time. The frontal positions at the upper and lower boundaries thus stay almost fixed during the time integration, as can be seen in Figs. 3(a) and 4(a). The strength of the front increases, as does the geostrophic wind v_g near the boundaries. The cross frontal circulation shown in Figs 4(c) and (d) shows that the vertical motion reaches its maximum value very close to the boundaries. Note that this is the actual vertical motion, not the pseudo vertical motion $\dot{\sigma}$ that appears in equations (2.19) - (2.22)

The results from the finite difference model, using a uniform 50 x 12 grid to cover the whole domain, are shown in Fig. 5. The boundary conditions are moved in with time, so that only the solution on the inner 30 x 12 gridpoints is shown in Fig. 5.

There is good general agreement with the Lagrangian solutions. There is some smoothing of the potential temperature gradient at the boundaries. This is partly because the staggered grid only holds values of θ a full grid length in from the boundary. A stretched grid near the boundary might give a sharper front. The maximum values of v_g are well captured. Fig.5(c) shows the horizontal cross-front wind with the basic deformation removed. The maximum values are reached in shallow layers near the upper and lower boundaries, and agree to within 0.5 ms^{-1} with those from the Lagrangian model. The largest difference is the underestimation of the maximum at the lower boundary in the finite difference model. The vertical velocity reaches its maximum values closer to the upper than the lower boundary. The largest values are within 0.5 cm s^{-1} of those predicted by the Lagrangian model. In the finite difference model there is an enhanced maximum and an extra minimum near the upper boundary, suggestive of a weak computational instability. The maximum near the lower boundary is underestimated.

A second case is illustrated in Fig. 6. The data used have a much stronger temperature stratification. This means that the fronts do not penetrate so far into the fluid and the vertical velocity will be smaller. The Lagrangian solution shown in Fig. 6(a) illustrates that no elements actually separate from the boundary. The potential temperature fields agree closely and there is little evidence of numerical smoothing. The vertical velocity fields also agree well, the maximum upward motion is the same in both solutions, though its position is slightly displaced between the two. The finite difference model produces an extra maximum of downward motion near the upper boundary, which appears to be a numerical error.

It would be desirable to compare the two methods more objectively by calculating difference fields. This is only useful if a much higher resolution can be used in the Lagrangian method. At presently affordable resolutions, the use of piecewise constant data in one method and grid-point approximation in the other makes objective comparison difficult.

In order to test the stability of the numerical method, and its ability to follow an inviscid discontinuous solution for a long

period, the problem was solved using the initial data in Fig. 3 and a deformation rate proportional to $\cos(\lambda t)$. The maximum reduction in cross section was a factor of 0.5, and the equations were integrated through five periods. The exact solution will oscillate in time with the strength of the discontinuity varying periodically. This behaviour is exactly reproduced by the Lagrangian model. The results after one and five cycles using the finite difference model are compared in Fig. 7. The differences are very small, despite the various smoothing devices used in the calculations and the difficulty of imposing the correct boundary conditions which causes the slight drift in the mean values.

4.2 Mountain flow

The governing equations are (2.13), (2.14), (2.16), (2.19) and (2.24)-(2.28). A similar problem was solved using a Lagrangian method by Cullen, Chynoweth and Purser, [13]. It was only possible to use a low resolution description of the flow because of the difficult computer logic and therefore quantitative details of this solution should not be compared with a high resolution finite difference calculation.

The main features of the solution are illustrated in Figs. 8(a) and 9(a). Fluid is flowing at $11ms^{-1}$ over a barrier 2000m high and 120 km wide. The elements are numbered. As fluid crosses the barrier the element tangent to the top of the barrier is split and its area gradually transferred from an upstream to a downstream position. The two parts of such elements are denoted A and B. The division into elements corresponds to contours of constant θ. Elements 4-10, 11-17, 18-24, 25-31 and 32-36 represent layers of constant θ. As time proceeds, fluid is blocked upstream for a period and then jumps to a new downstream position. The slopes of the lines of constant θ at low levels upstream are reduced. There is a hydrostatic pressure difference of 8 pascals across the barrier. Element 28 is brought down to the surface behind the barrier, implying the descent of less dense and therefore warmer air. There is very little effect on the fluid higher up than the barrier height. There is a net displacement of lower level fluid from left to right. Equation (2.24) shows that this will be compensated by a reduction in the values of v_g . The effect is much smaller at upper levels.

The initial data for the finite difference model is shown in Figs.8(b) and (c). It is chosen so that the θ and v_g distributions are similar to the Lagrangian data and the barrier has the same height and cross sectional area. The output uses physical height rather than pressure as a vertical coordinate and extends up to 12km, though the model itself extends higher than this. The irregularities in the θ field over the mountain top result from the interpolation. A uniform 80 x 10 grid is used, with a horizontal

grid length of 31 km.

The finite difference solution after 12 hours is shown in Figs. 9(b) - (e). The θ field above the mountain top has correctly been translated with little change. Cold air is trapped to the left of the mountain and the change of slope of the upstream isentropes is predicted. The cold air crossing the mountain top loses its identity due to numerical mixing and there is no downstream cold air corresponding to element 36B. The dragging of warmer air down on the lee side is correctly predicted. There are numerical errors at the gridpoint directly over the mountain top. The v_g field, Fig. 9(c), shows the advection of the main maximum towards the mountain barrier. The results at low levels for the u and w fields, Figs. 9(d) and (e), show the attempt of the finite difference model to model the singular behaviour of the Lagrangian solution. At the lowest layer of gridpoints upstream the flow is blocked and v_g increases according to equation (2.24). At the second level the flow is accelerated to bring fluid across the barrier and v_g decreases. Above the second level there is little effect on the θ field but there are some oscillations in the v_g field. Downstream of the barrier at low levels there is a 'start vortex', caused by the vertical expansion of the column of air directly above the mountain top at the initial time. The upstream barrier jet reaches a peak of $9ms^{-1}$ compared with $15ms^{-1}$ deduced at the left hand boundary of element 36 in the Lagrangian solution. The u field does not deviate from its basic value of $11ms^{-1}$ by more than $1ms^{-1}$ except near the barrier, where it reaches $50ms^{-1}$, and at some gridpoints at the top of the model, not shown in Fig. 9(d). The vertical velocity shown is again the true physical vertical motion, not the pseudo-vertical velocity $\dot{\sigma}$. There are values up to $6cms^{-1}$ above the barrier extending up to the top of the model which are caused by numerical errors. Values near the barrier reach $1ms^{-1}$.

The pressure difference across the mountain at the surface is 2.5 pascals. This is less than that deduced from the Lagrangian model, but the latter value may be increased by the simple block used to represent the barrier and the low resolution of the rest of the calculation.

5. SUMMARY

These results suggest that a carefully designed implicit finite difference algorithm can represent discontinuous Lagrangian solutions representing atmospheric fronts, and can follow a solution in which fronts are formed and dissipated several times. It is also possible to approximate a highly singular solution describing flow over a mountain barrier. It is not clear in what sense "convergence" is meaningful in this case. It would be highly desirable to establish theoretically under what conditions the iteration strategy, which had to be developed empirically, does in fact converge to the desired solutions. The theoretical tools necessary to do this are some way off.

ACKNOWLEDGMENTS

The author wishes to thank Dr. S. Chynoweth for providing the solutions of the Lagrangian model in advance of publication, Dr. J. Norbury for advice in designing the finite difference procedure and Mr. C.A. Parrett and Mr. R. Bowles for programming assistance.

REFERENCES

1. N.J. Norton, J.C.McWilliams, and P.R.Gent, J. Comput. Phys., 67, 439 (1986).
2. A. Eliassen, Geofys. Publikusjoner, 17, No. 3 (1948).
3. B.J. Hoskins, J. Atmos. Sci., 32, 233 (1975).
4. M.J.P. Cullen and R.J. Purser, J. Atmos. Sci., 41, 1477 (1984).
5. M.J.P. Cullen, J. Norbury, R.J. Purser and G.J. Shutts, Quart. J. Roy. Meteor. Soc., 113, 735 (1987).
6. G.J. Shutts, J. Atmos. Sci., 44, 2018 (1987).
7. S. Chynoweth, Ph. D. thesis, Dept. Maths., Univ. of Reading, U.K. (unpublished).
8. A.V.Pogorelov, Monge-Ampere Equations of Elliptic Type (Noordhoff, Groningen, 1964).

9. A. Arakawa, J. Comput. Phys., 1, 119 (1966).
10. B.J. Hoskins and F.P. Bretherton, J. Atmos. Sci., 29, 11 (1972).
11. R.M. Beam and R.F. Warming, J. Comput. Phys., 22, 87 (1976).
12. P.C. Meek and J. Norbury, SIAM J. Numer. Anal., 21, 883 (1984).
13. M.J.P. Cullen, S. Chynoweth and R.J. Purser. Quart. J. Roy. Meteor. Soc., 113, 163 (1987).
14. W. Blumen, J.Atmos. Sci., 38, 1100 (1981).
15. M.J.P.Cullen, Quart. J. Roy. Meteor. Soc., 109, 565 (1983).
16. J.Glimm, Commun. Pure Appl. Math., 18, 697 (1965).

List of figures

Fig. 1 Arrangement of variables on grid in (x,z) plane.

Fig. 2 Construction of approximation to equation (3.23) over variable terrain height.

Fig. 3 Initial data for front formulation, 2°C temperature difference in vertical.
(a) Element distribution for Lagrangian method, (b) potential temperature (°C), (c) Geostrophic wind (ms^{-1}).

Fig. 4 Solutions at t = 0.5 using Lagrangian model
(a) Element distribution,
(b) Potential temperature (°K), (c) Geostrophic wind (ms^{-1}),
(d) Horizontal cross-front velocity (ms^{-1}),
(e) Vertical velocity (cms^{-1}).

Fig. 5 Solutions at t = 0.5 using finite difference model,
(a) Potential temperature (°K), (b) geostrophic wind (ms^{-1}),
(c) Horizontal cross front velocity (ms^{-1}), (d) vertical velocity (cms^{-1}).

Fig. 6 Solutions at t= 0.5 for front formation, 10°C temperature difference in vertical.
(a) Element distribution for Lagrangian method; (b) potential temperature (°C), Lagrangian method; (c) Potential temperature (°C), finite difference method; (d) vertical velocity (cms^{-1}), Lagrangian method; (e) vertical velocity (cms^{-1}) finite difference method.

Fig. 7 Solutions for periodic frontal deformation. (a) Potential

temperature (°C), 1st cycle solid lines, 5th cycle dashed lines, maximum compression; (b) Potential temperature (°C) !st cycle solid lines, 5th cycle dashed lines, maximum expansion.

Fig. 8 Solutions for flow over mountain ridge. Initial data : (a) Element distribution for Lagrangian method; (b) potential temperature(°K); (c) geostrophic wind (ms^{-1}).

Fig. 9 Solutions for flow over mountain ridge after 12 hours. (a) Element distribution for Lagrangian method; (b) potential temperature (°K), finite difference method; (c) geostrophic wind (ms^{-1}); (d) cross mountain velocity (ms^{-1}); (e) vertical velocity (cms^{-1}).

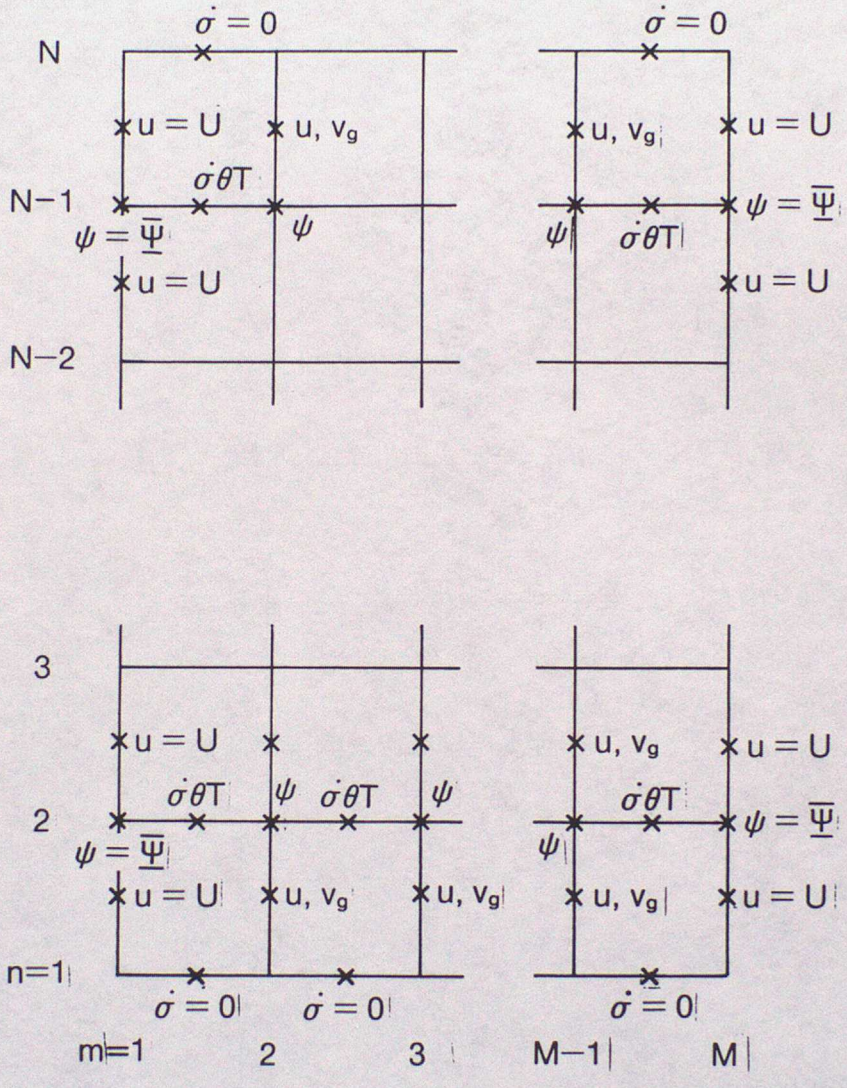
N
N−1
N−2
$\dot{\sigma} = 0$
u = U
u, v_g
$\dot{\sigma}\theta T$
$\psi = \overline{\Psi}$
ψ
u = U
$\dot{\sigma} = 0$
u, v_g
u = U
ψ
$\dot{\sigma}\theta T$
$\psi = \overline{\Psi}$
u = U
3
2
n=1
u = U
$\dot{\sigma}\theta T$
ψ
$\dot{\sigma}\theta T$
ψ
$\psi = \overline{\Psi}$
u = U
u, v_g
u, v_g
$\dot{\sigma} = 0$
$\dot{\sigma} = 0$
m=1
2
3
u, v_g
u = U
$\dot{\sigma}\theta T$
ψ
$\psi = \overline{\Psi}$
u, v_g
u = U
$\dot{\sigma} = 0$
M−1
M

Fig. 1

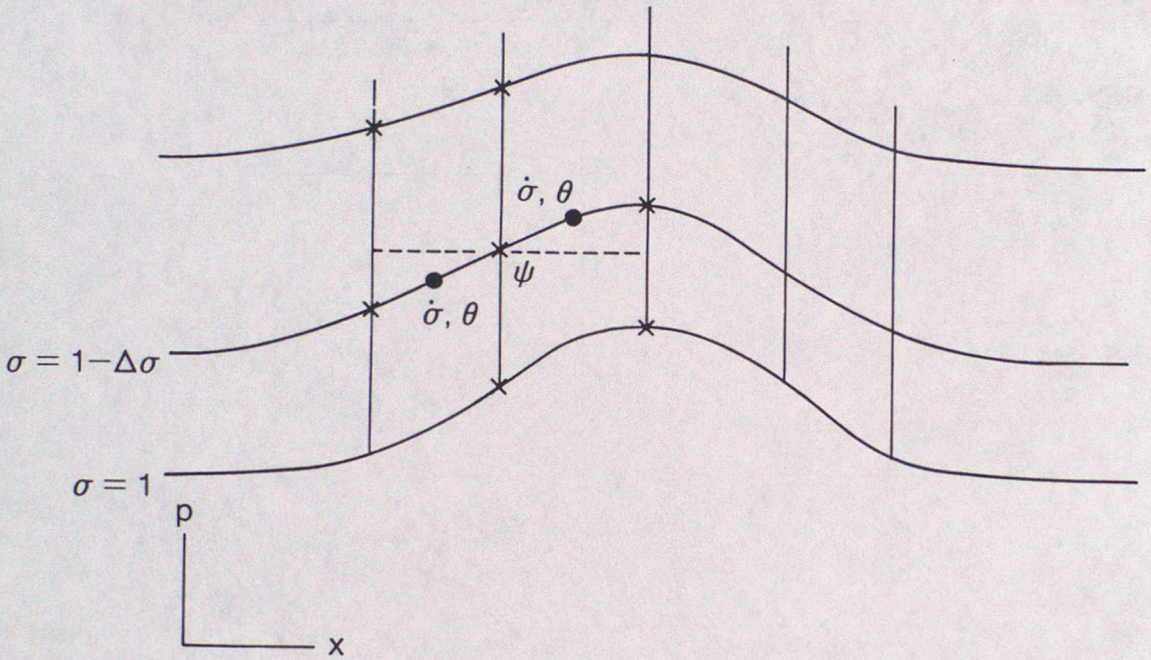
$\dot{\sigma}, \theta$
ψ
$\dot{\sigma}, \theta$
$\sigma = 1-\Delta\sigma$
$\sigma = 1$
p
x

Fig. 2

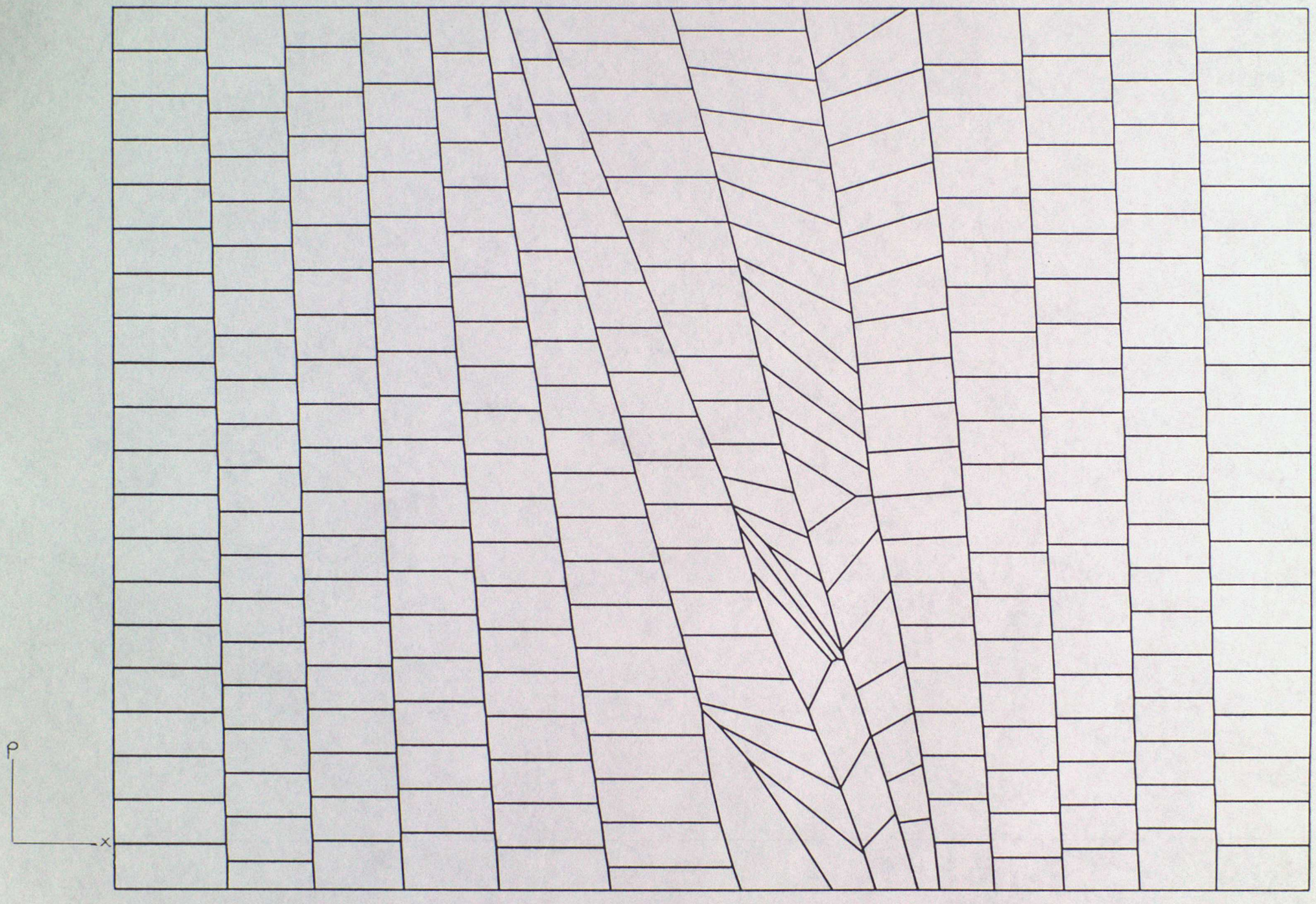

Fig. 3a

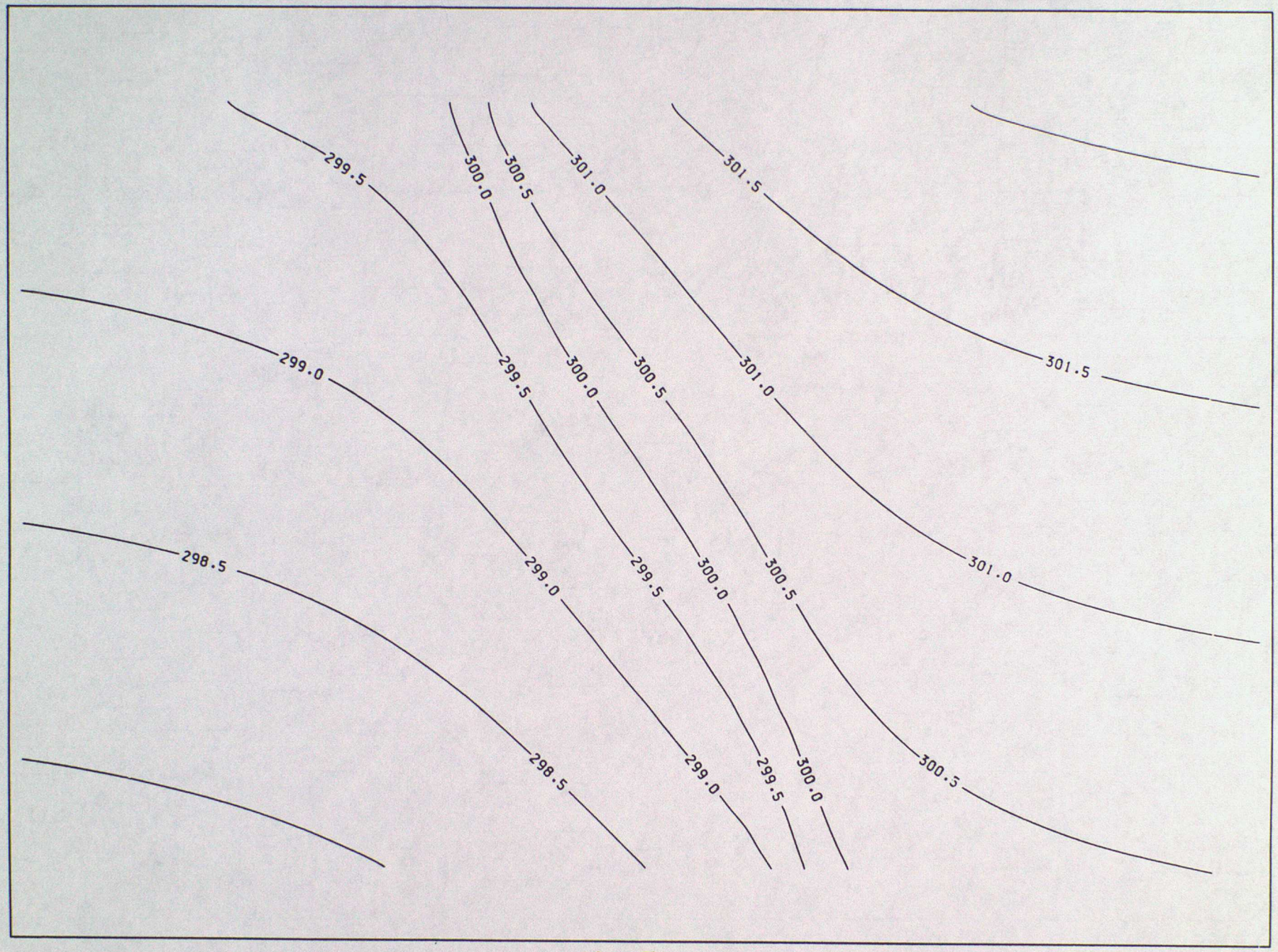

Fig. 3b

Fig. 3c

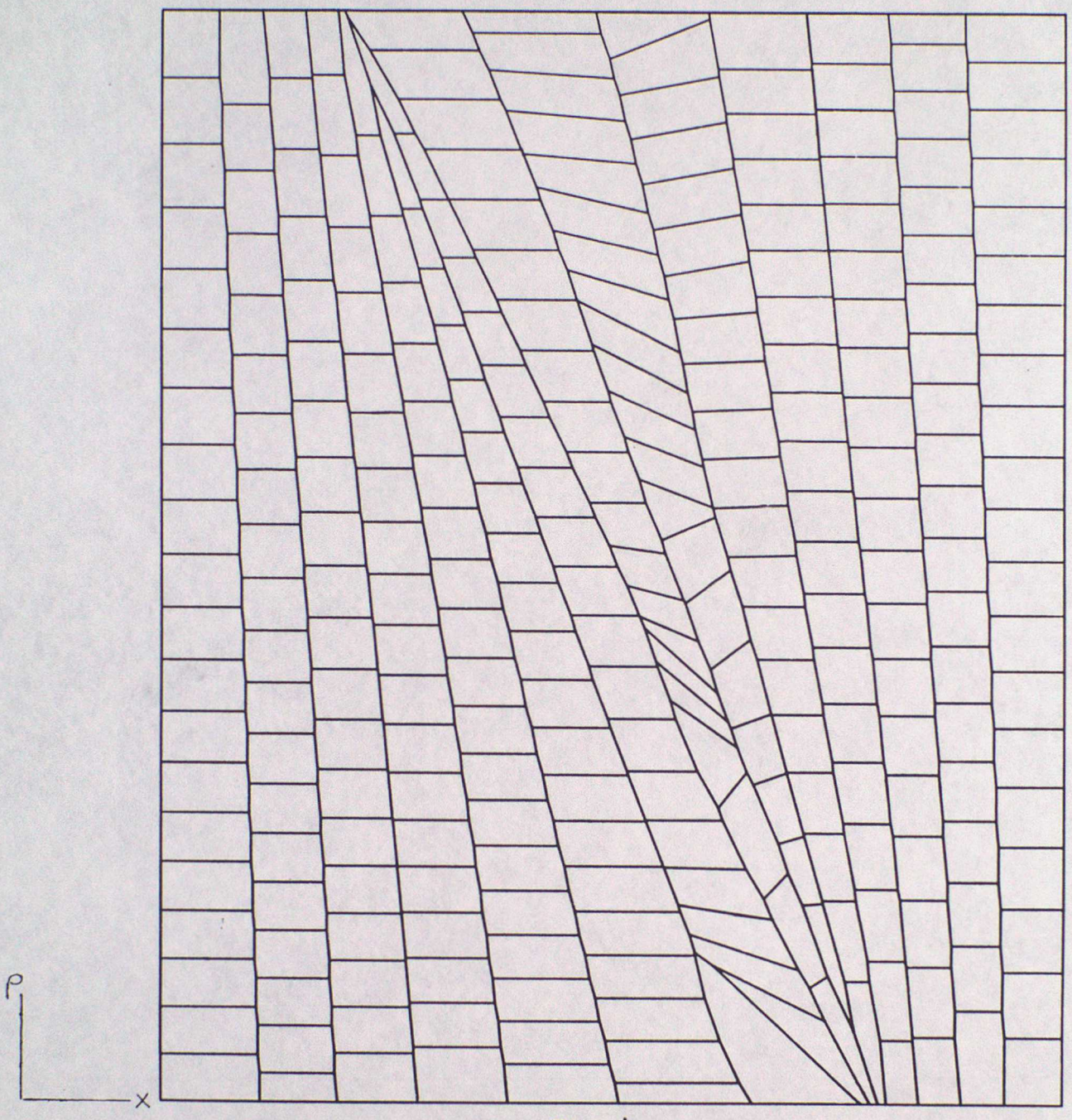

Fig. 4a

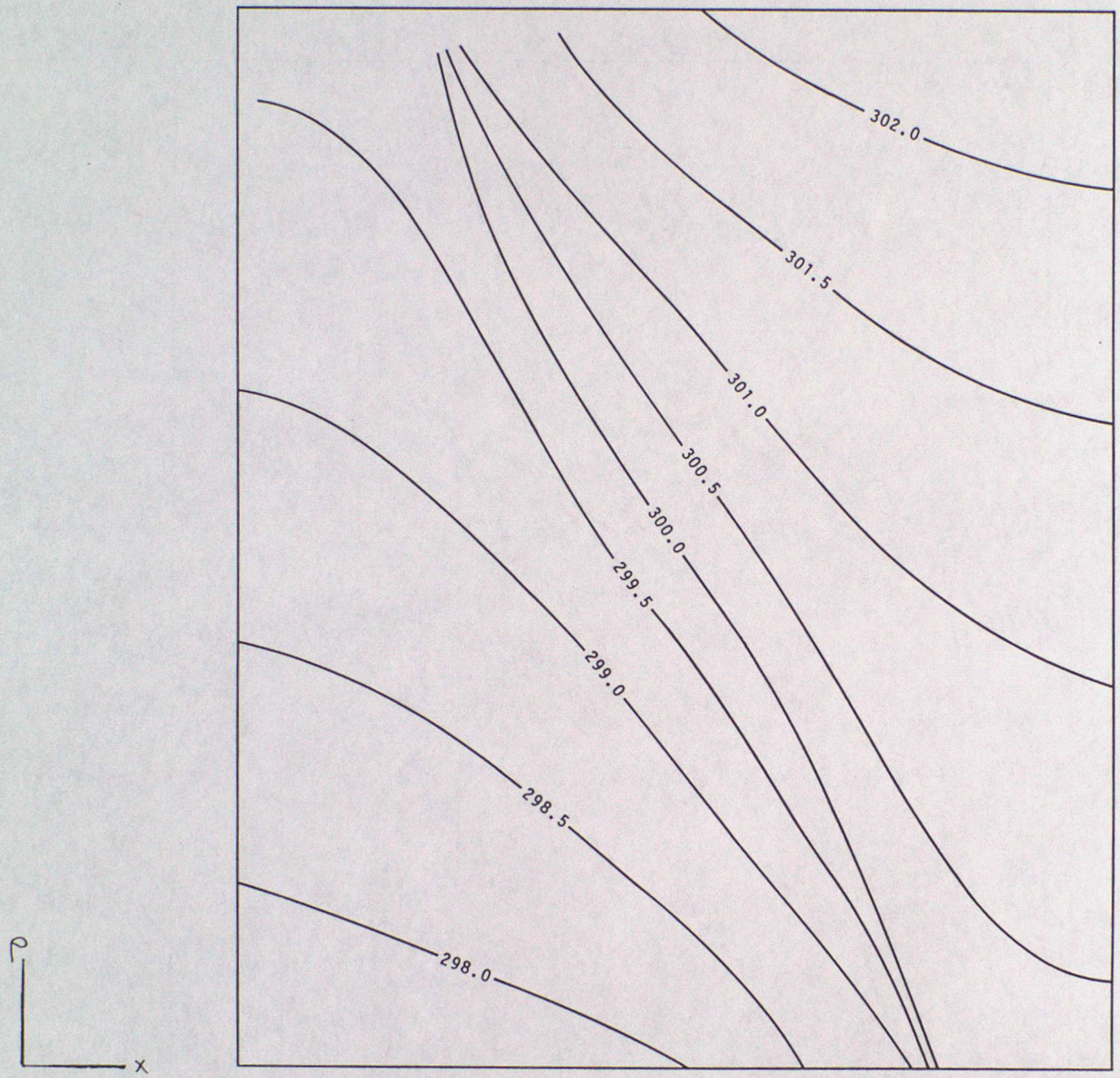

Fig. 4b

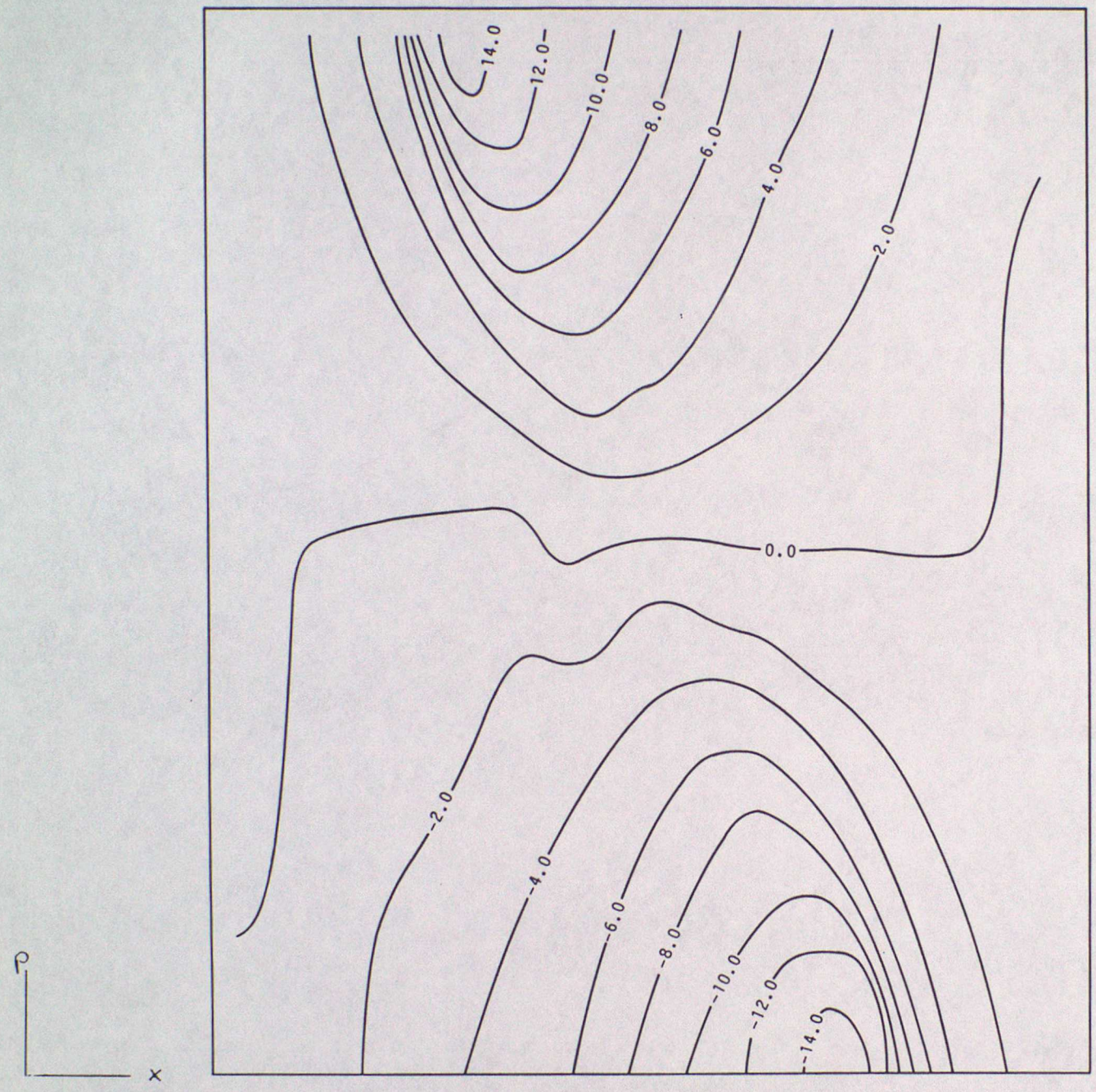

Fig. 4c

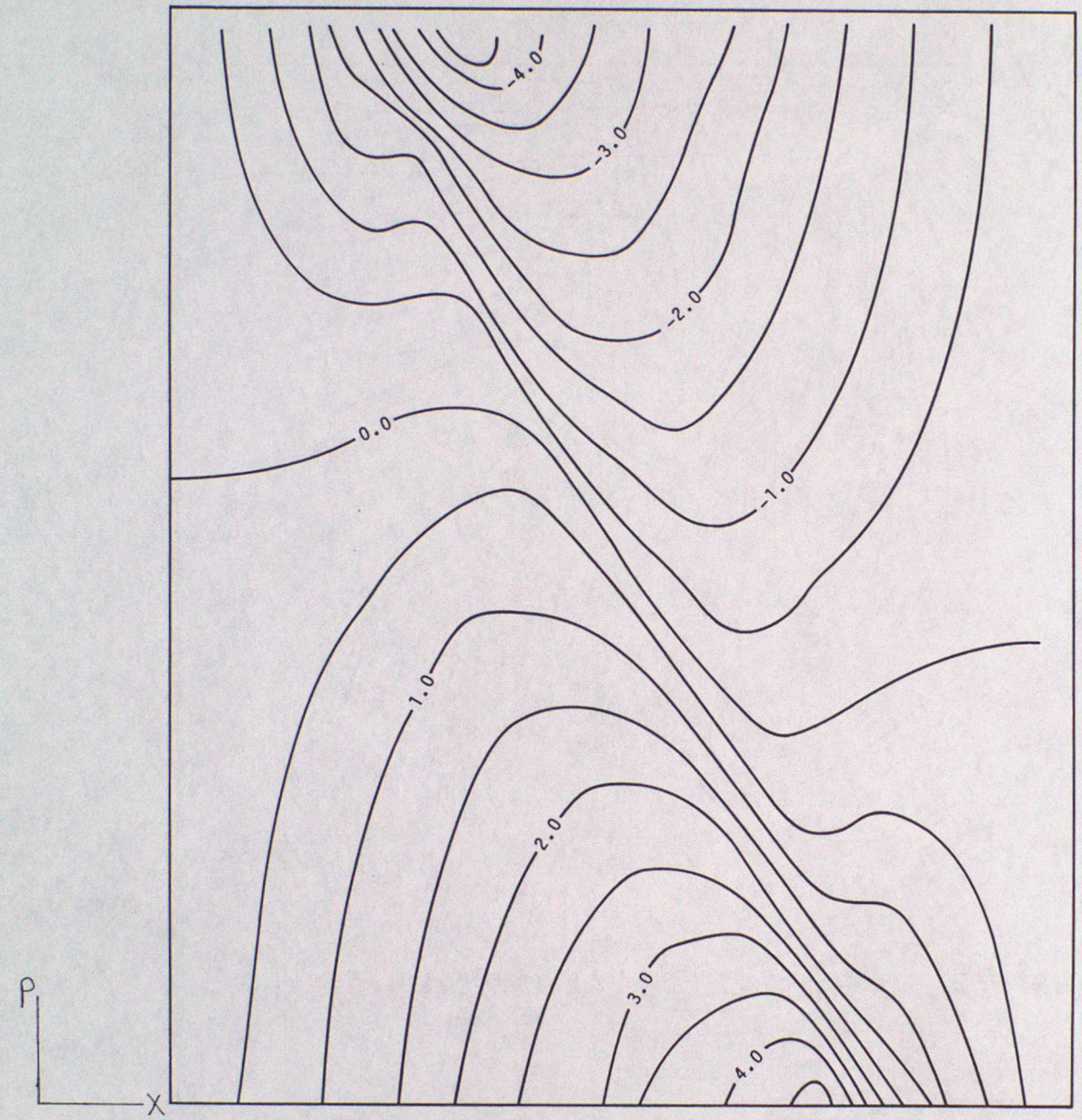

Fig. 4d

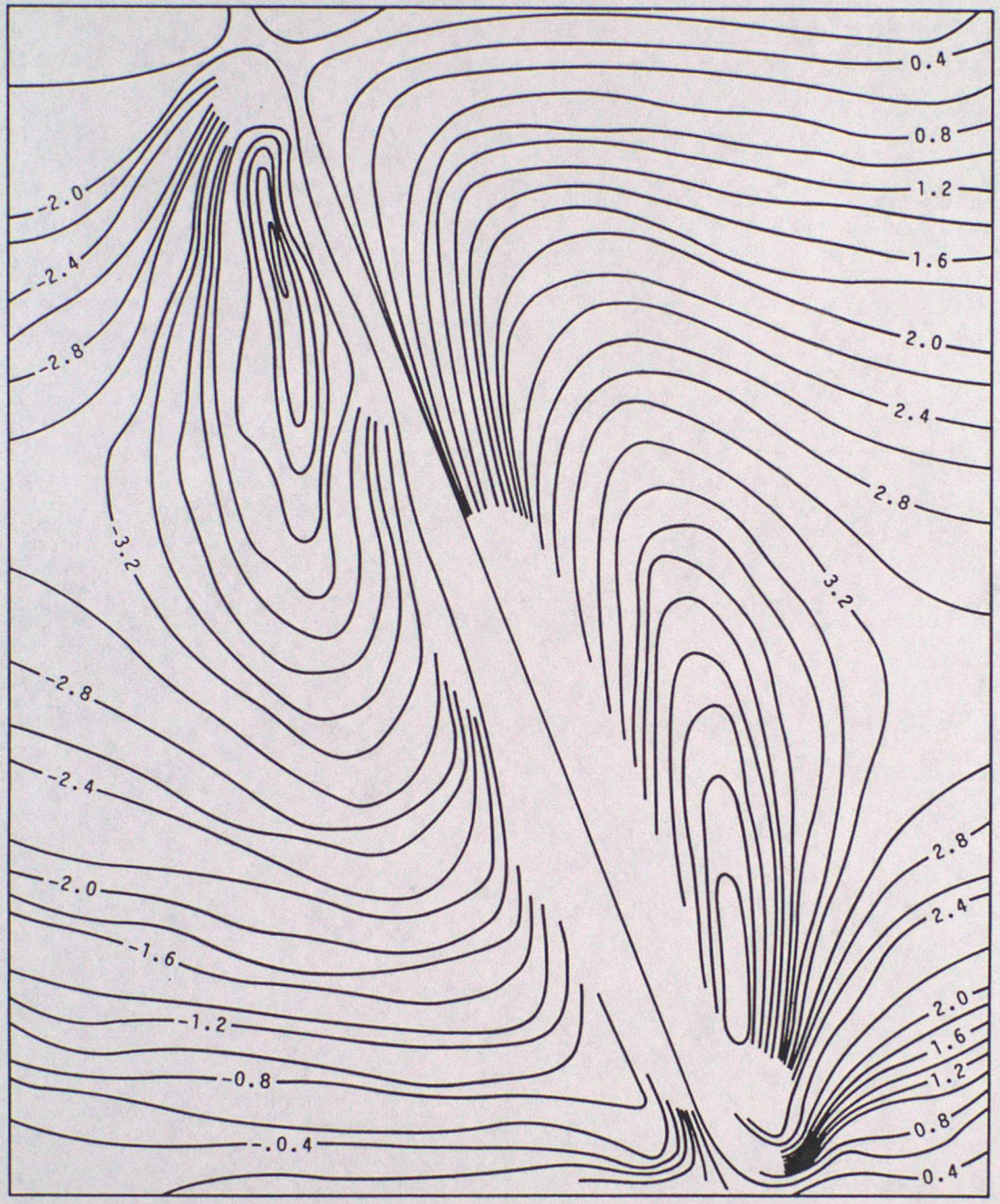
0.4
0.8
1.2
1.6
2.0
2.4
2.8
3.2
-2.0
-2.4
-2.8
-3.2
-2.8
-2.4
-2.0
-1.6
-1.2
-0.8
-.0.4
2.8
2.4
2.0
1.6
1.2
0.8
0.4
P
X

Fig. 4e

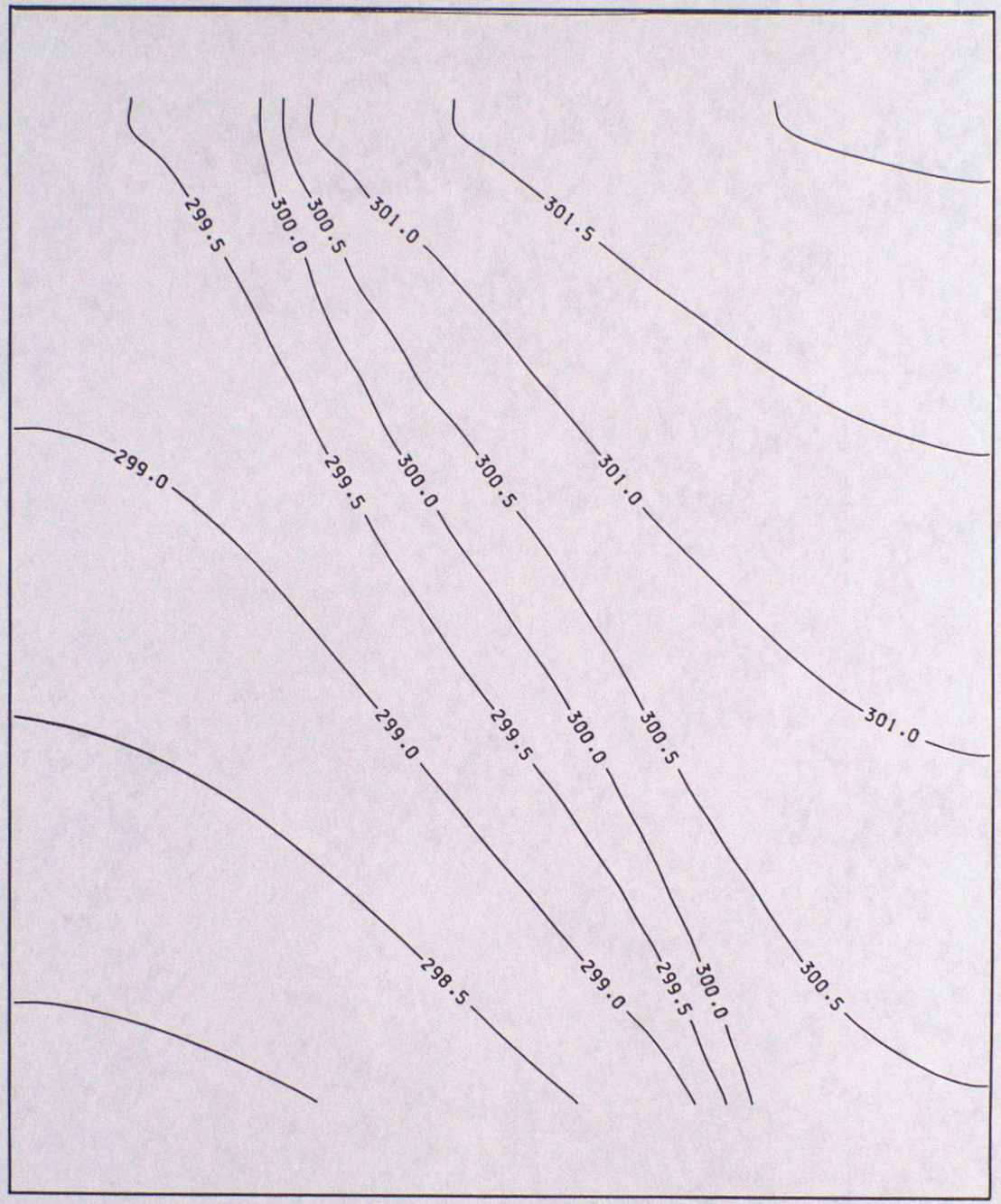
299.5
300.0
300.5
301.0
301.5
299.0
299.5
300.0
300.5
301.0
299.0
299.5
300.0
300.5
298.5
299.0
299.5
300.0
300.5
ρ
X

Fig. 5a

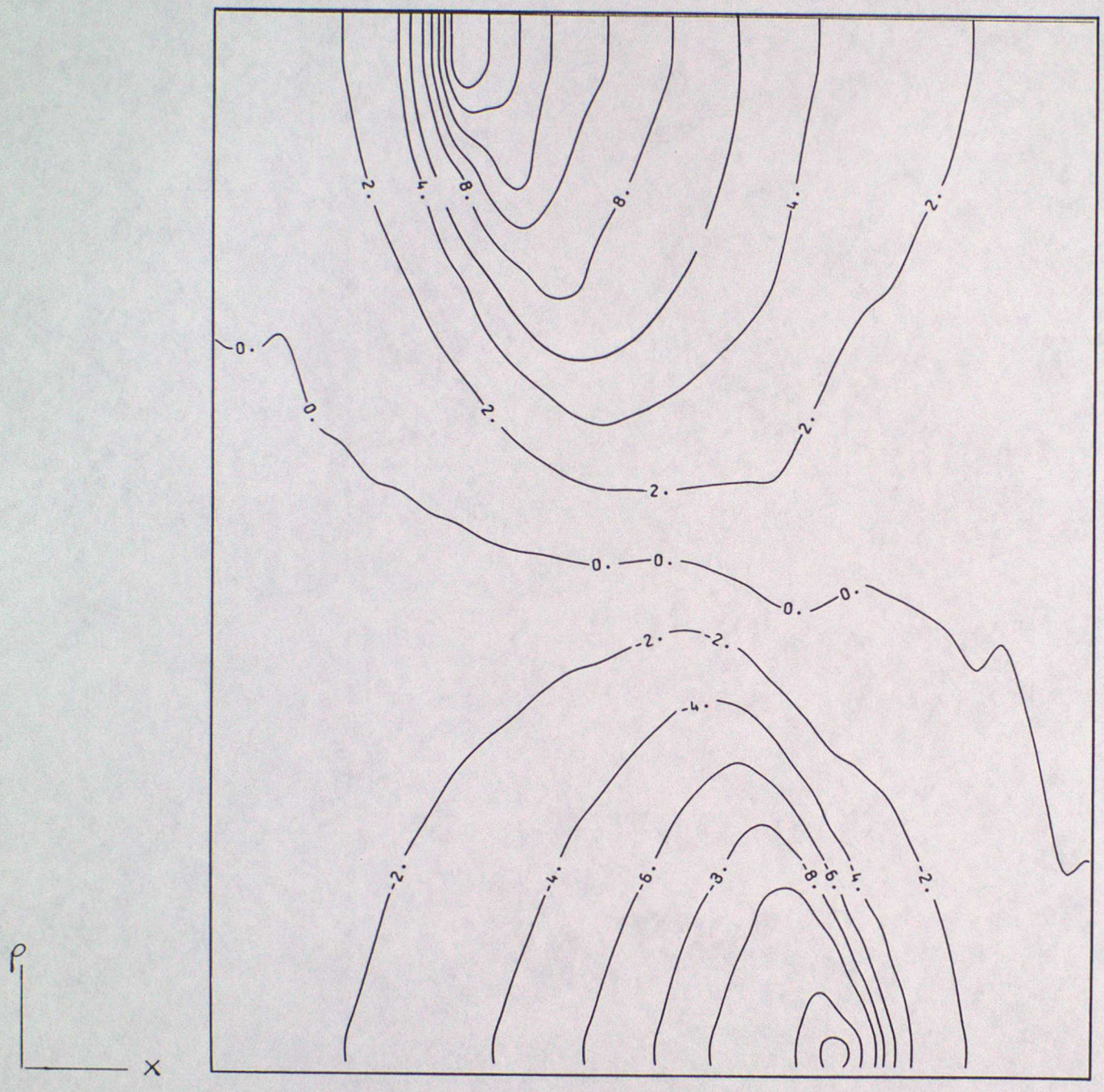

Fig. 5b

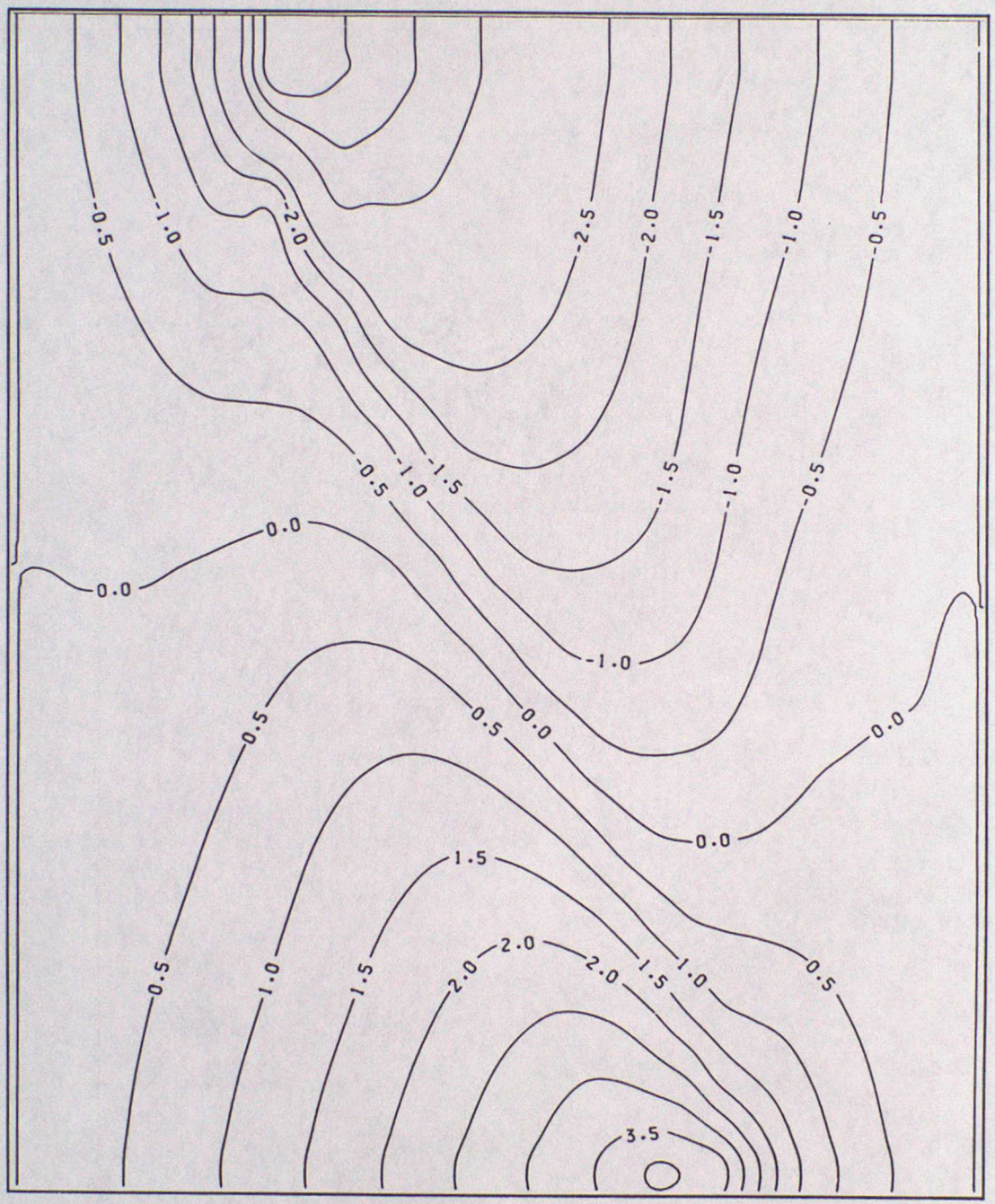
-0.5
-1.0
-2.0
-2.5
-2.0
-1.5
-1.0
-0.5
-0.5
-1.0
-1.5
-1.5
-1.0
-0.5
0.0
0.0
-1.0
0.5
0.5
0.0
0.0
0.0
1.5
0.5
1.0
1.5
2.0
2.0
2.0
1.5
1.0
0.5
3.5
ρ
X

Fig. 5c

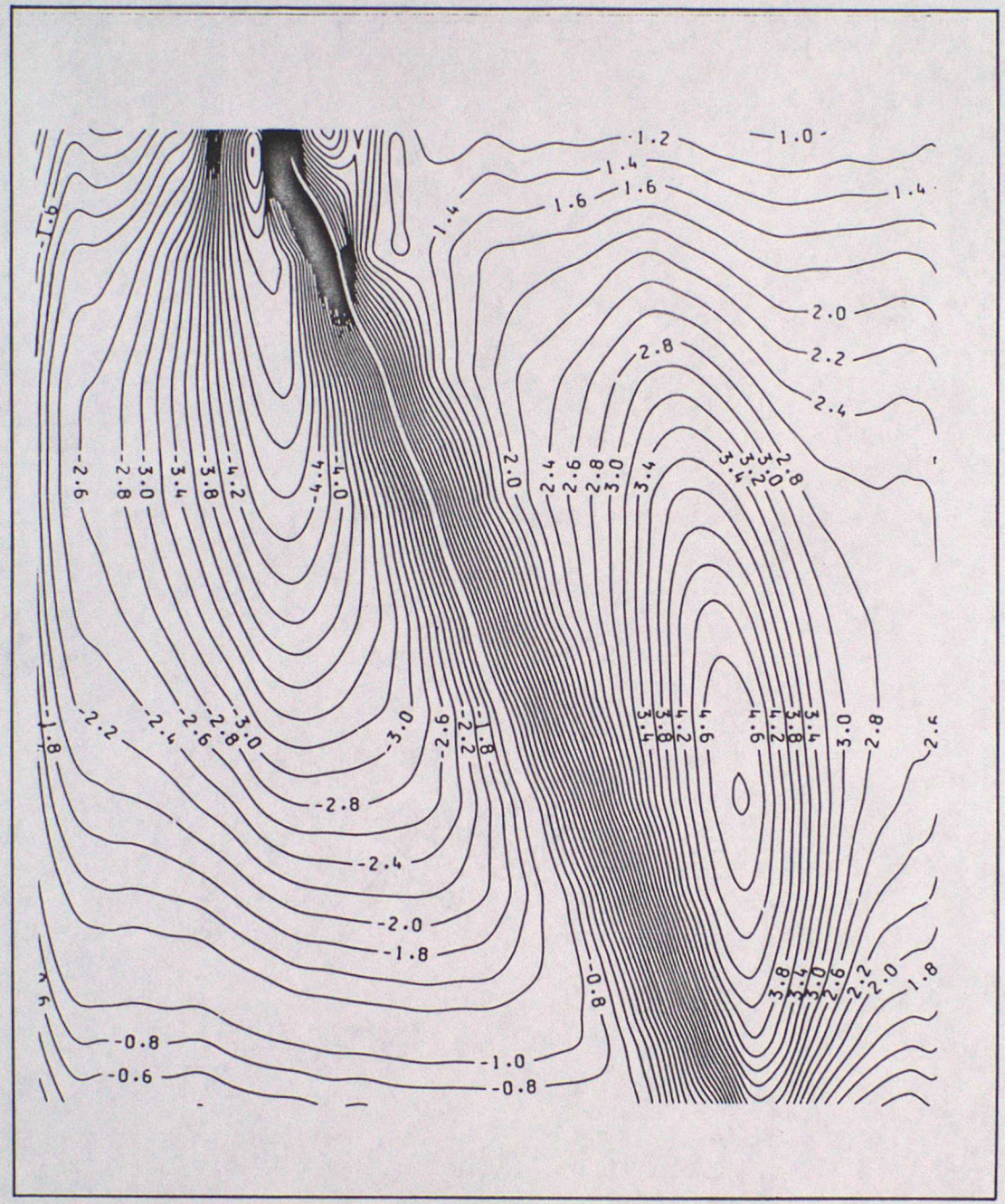
-1.2
-1.0
1.4
1.6
1.6
1.4
-1.6
2.0
2.8
2.2
2.4
-2.6
-2.8
-3.0
-3.4
-3.8
-4.2
-4.4
-4.0
2.0
2.4
2.6
2.8
3.0
3.4
3.4
3.2
3.0
2.8
-1.8
2.2
-2.4
-2.6
-2.8
-3.0
-3.0
-2.6
-2.2
-1.8
3.4
3.8
4.2
4.6
4.6
4.2
3.8
3.4
3.0
2.8
2.4
-2.8
-2.4
-2.0
-1.8
-0.8
3.8
3.4
3.0
2.6
2.2
2.0
1.8
-0.8
-1.0
-0.6
-0.8
ρ
X

Fig. 5d

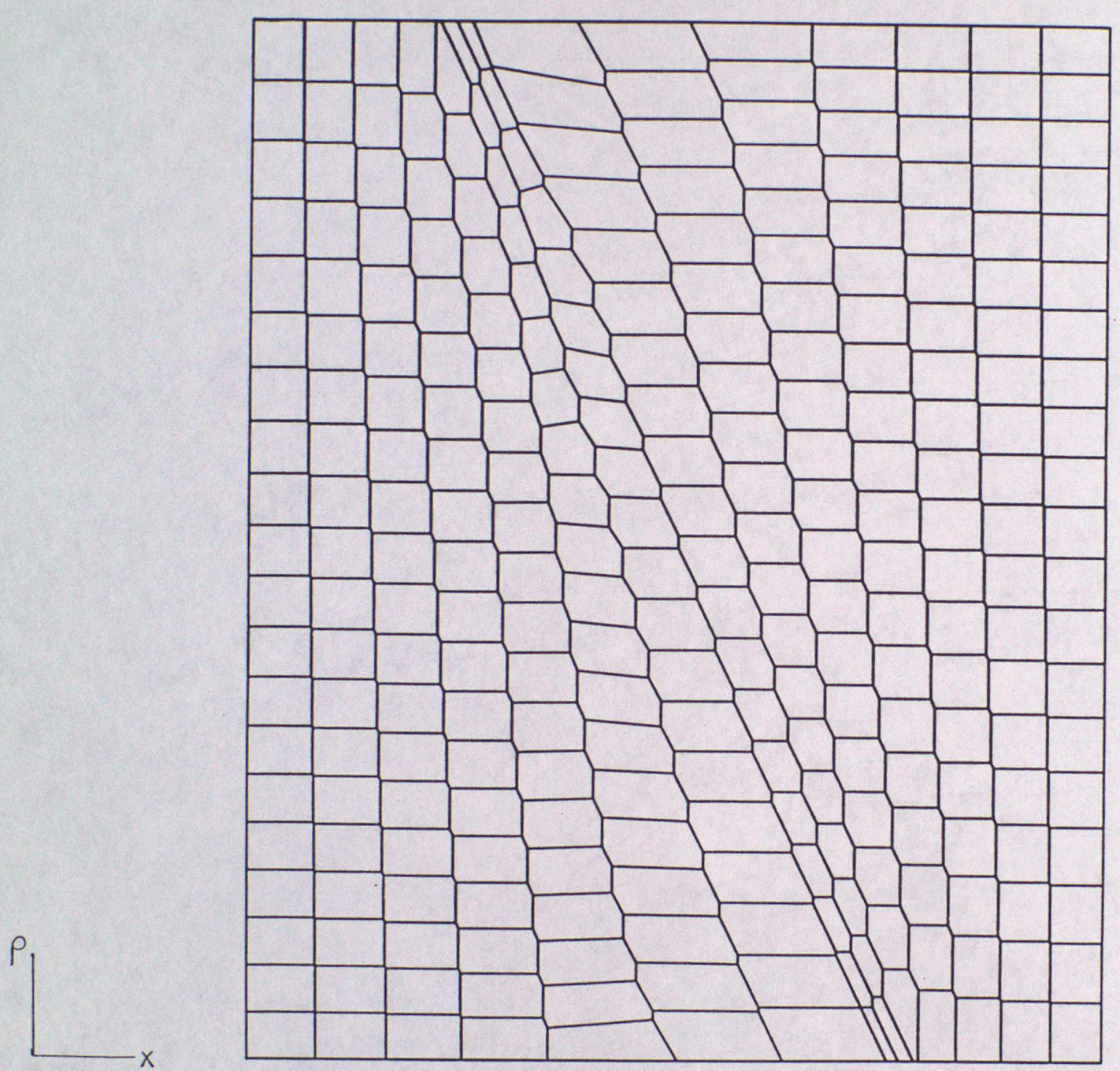

Fig. 6a

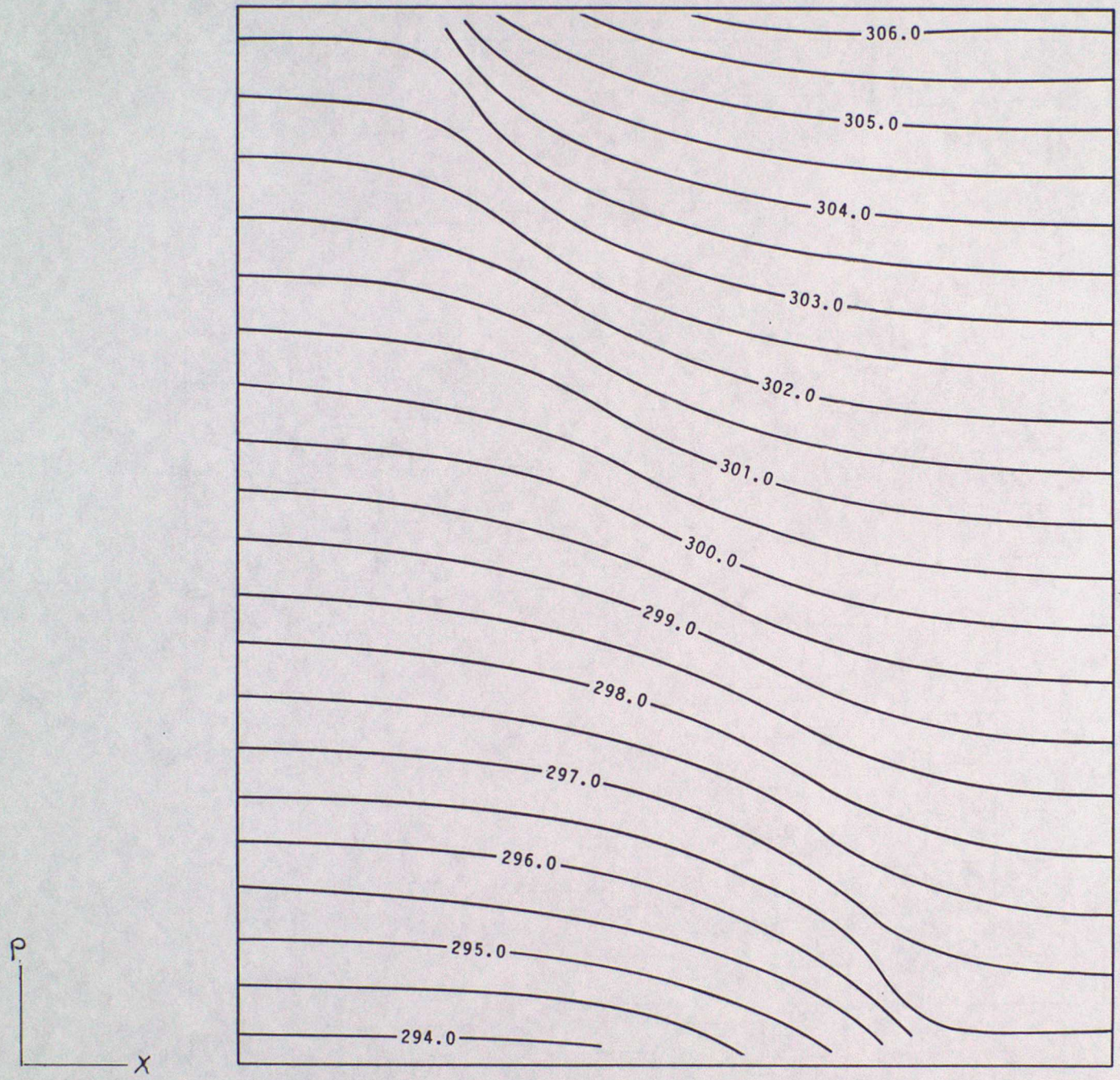
306.0
305.0
304.0
303.0
302.0
301.0
300.0
299.0
298.0
297.0
296.0
295.0
294.0
P
X

Fig. 6b

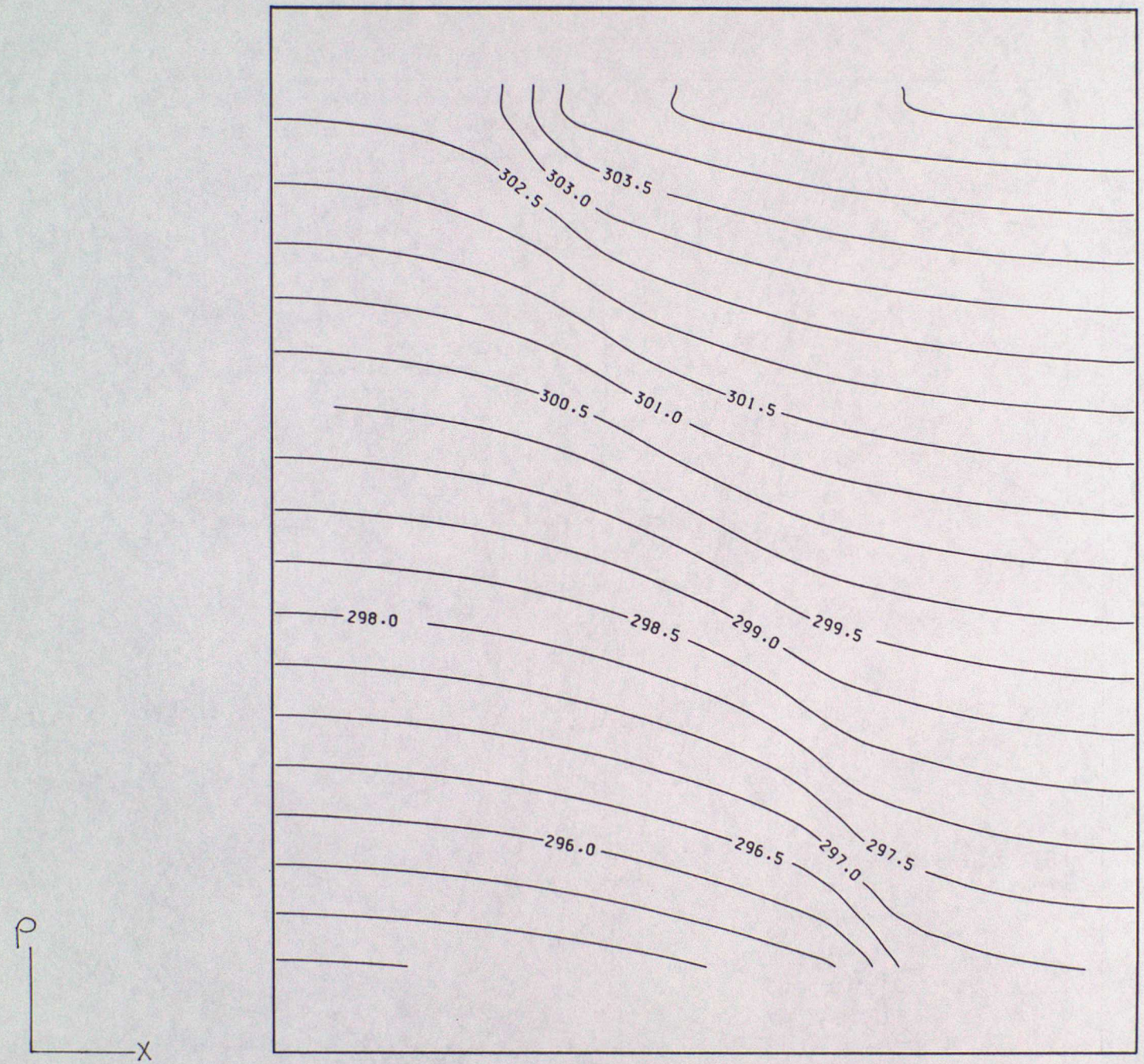
303.5
303.0
302.5
301.5
301.0
300.5
299.5
299.0
298.5
298.0
297.5
297.0
296.5
296.0
P
X

Fig. 6c

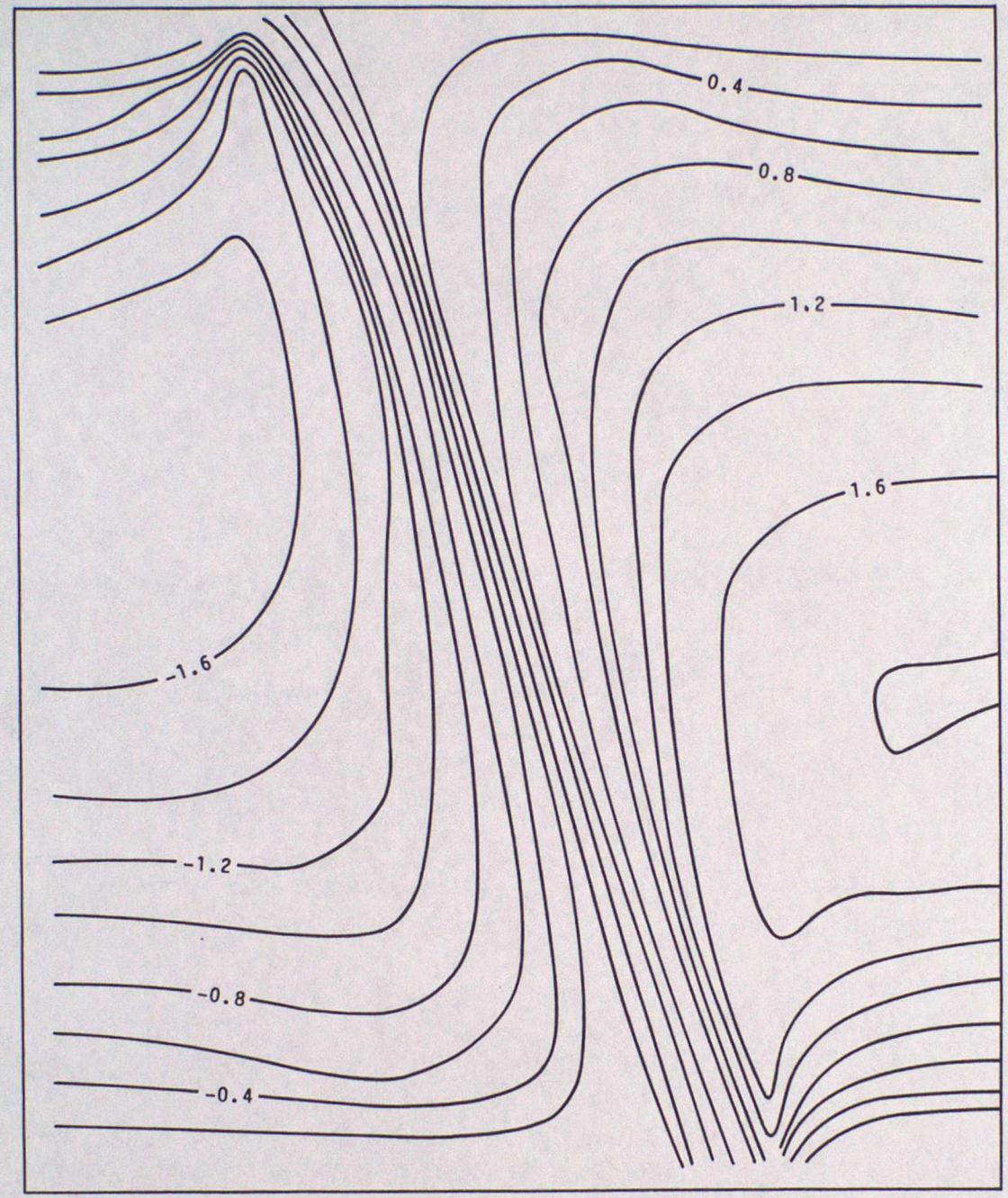

Fig. 6d

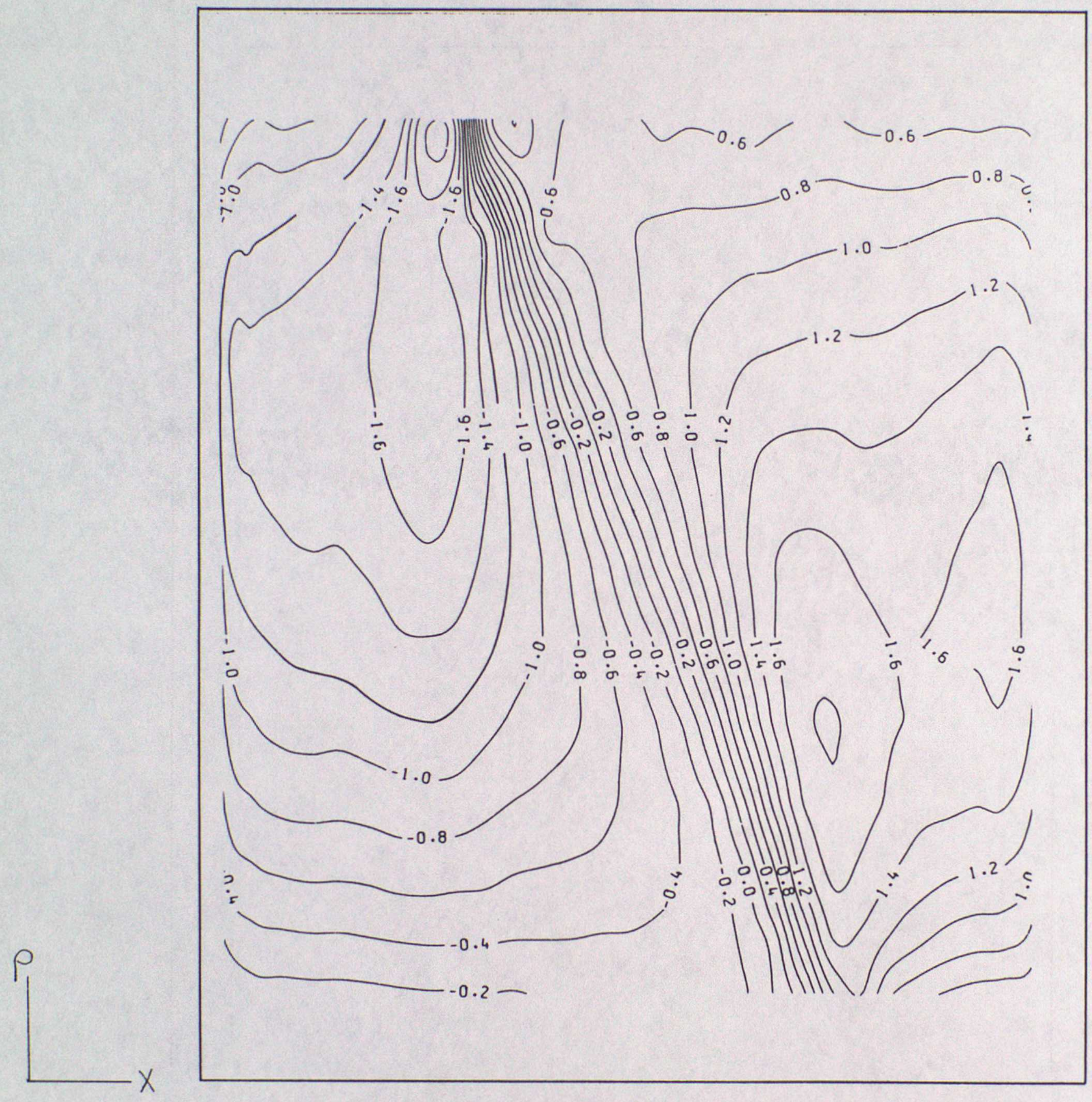

Fig. 6e

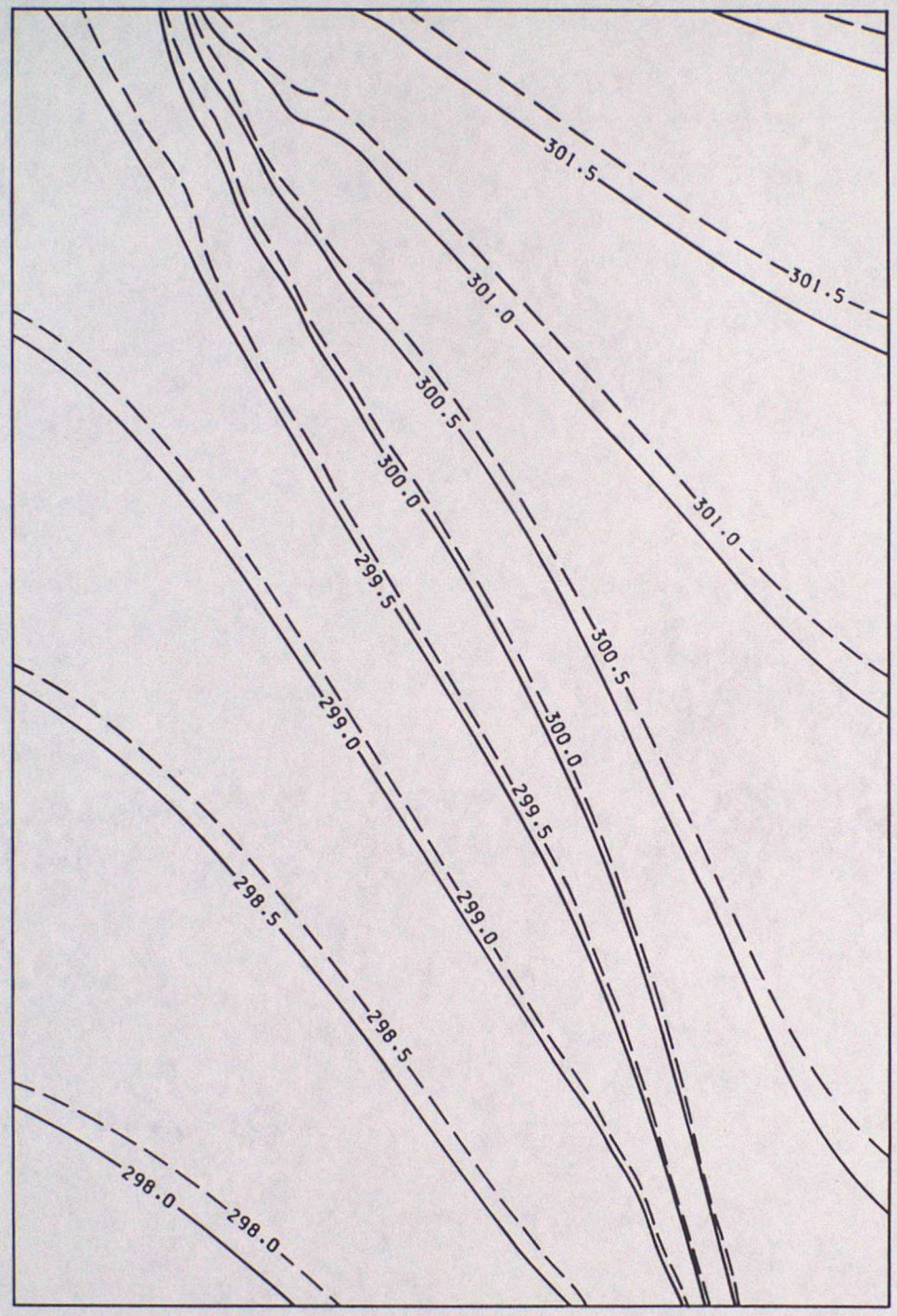
301.5
301.5
301.0
301.0
300.5
300.5
300.0
300.0
299.5
299.5
299.0
299.0
298.5
298.5
298.0
298.0
P
X

Fig. 7a

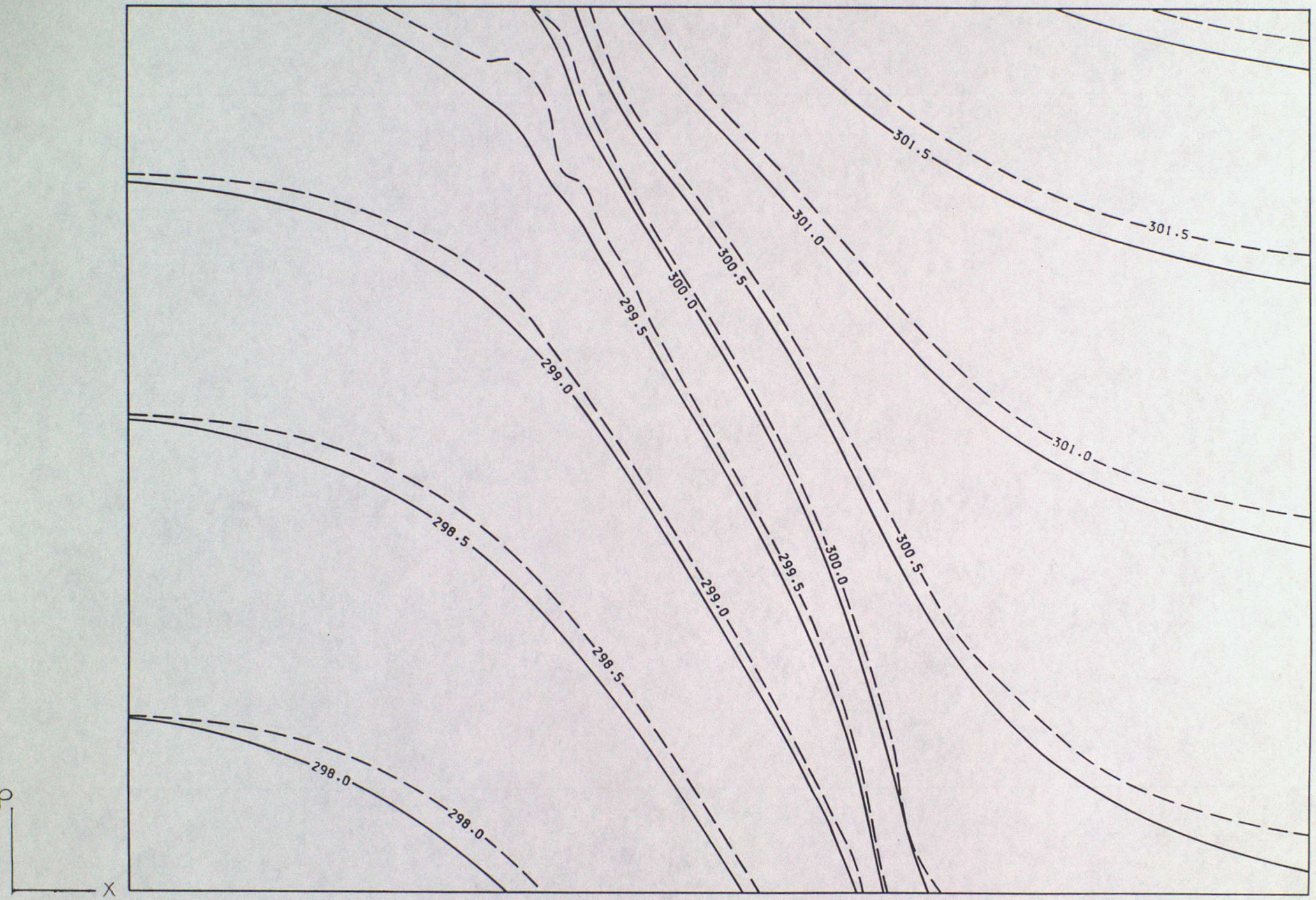
301.5
301.5
301.0
300.5
300.0
299.5
299.0
301.0
300.5
300.0
299.5
299.0
298.5
298.5
298.0
298.0
ρ
X

Fig. 7b

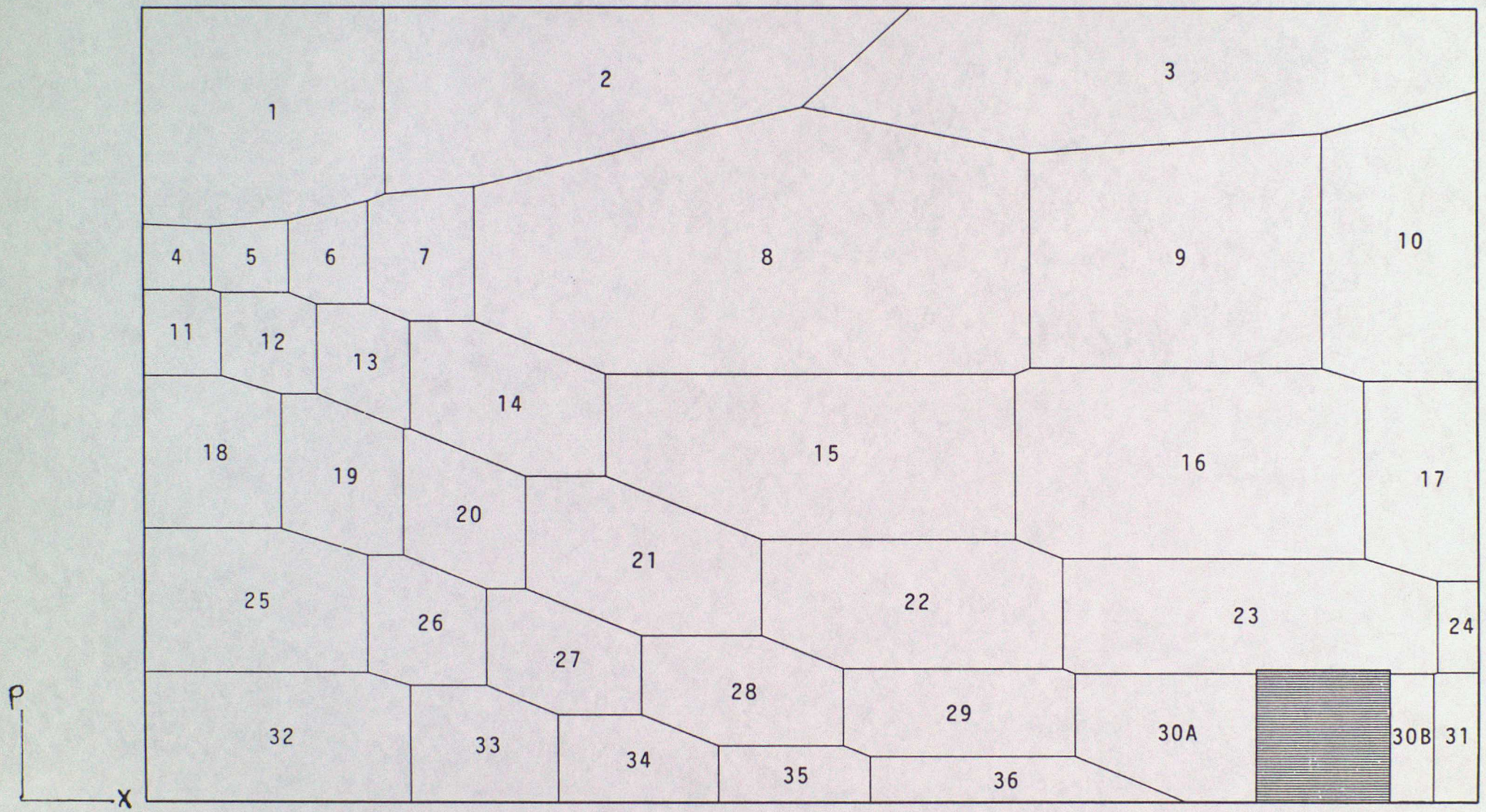
1
2
3
4
5
6
7
8
9
10
11
12
13
14
15
16
17
18
19
20
21
22
23
24
25
26
27
28
29
30A
30B
31
32
33
34
35
36
P
X

Fig. 8a

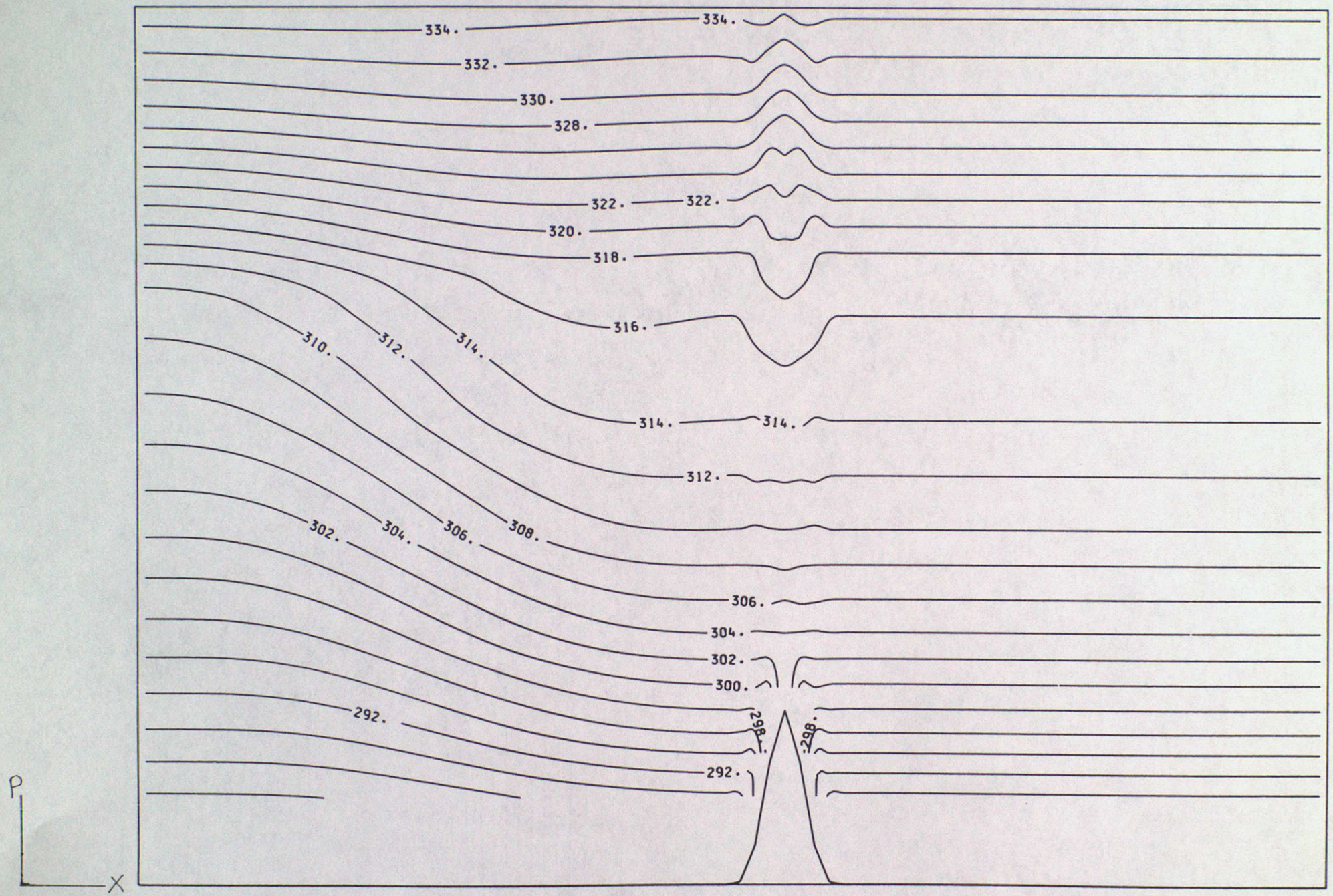
334.
334.
332.
330.
328.
322.
322.
320.
318.
316.
310.
312.
314.
314.
314.
312.
302.
304.
306.
308.
306.
304.
302.
300.
292.
298.
298.
292.
P
X

Fig. 8b

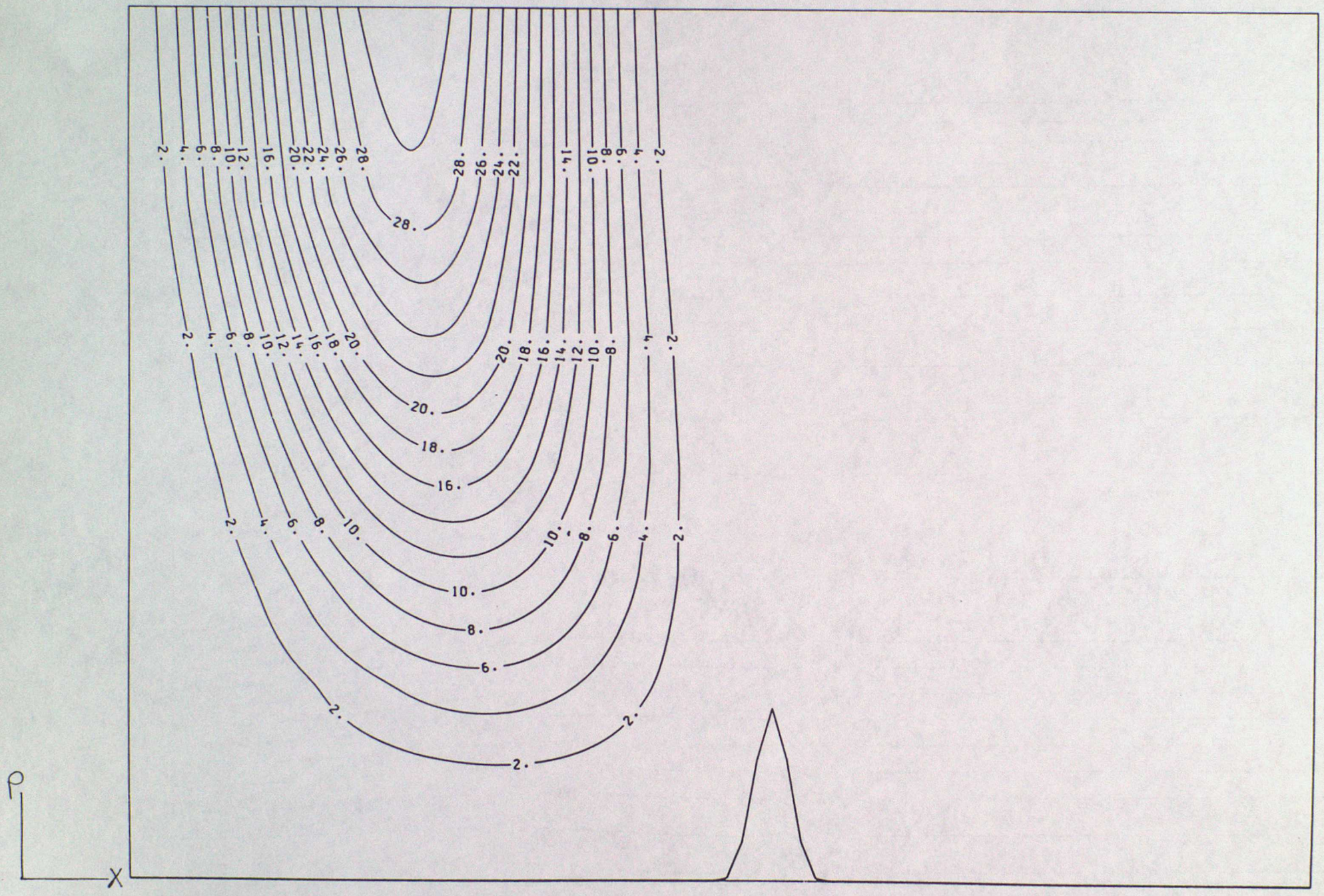

Fig. 8c

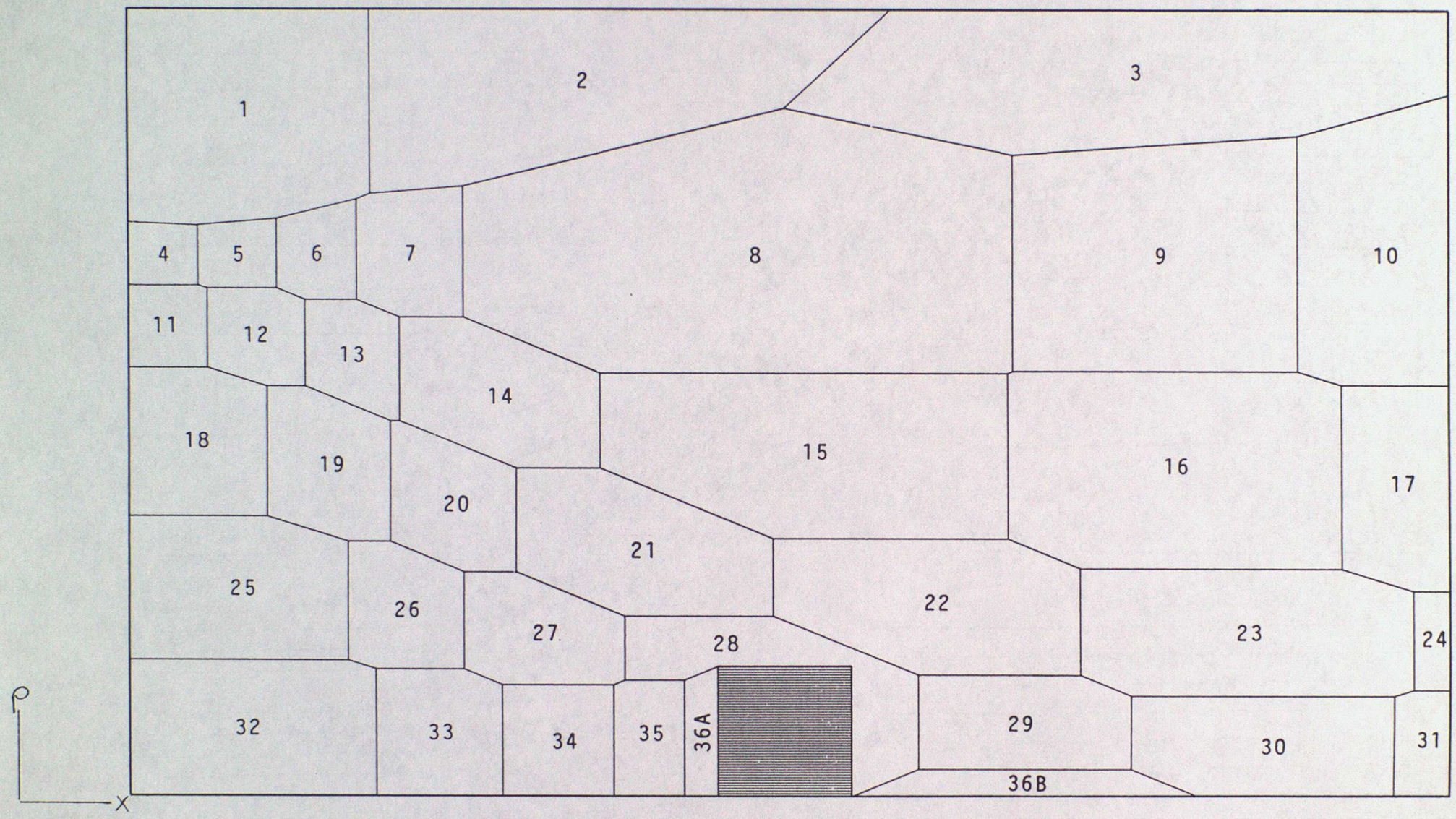
1
2
3
4
5
6
7
8
9
10
11
12
13
14
15
16
17
18
19
20
21
22
23
24
25
26
27
28
29
30
31
32
33
34
35
36A
36B
X

Fig. 9a

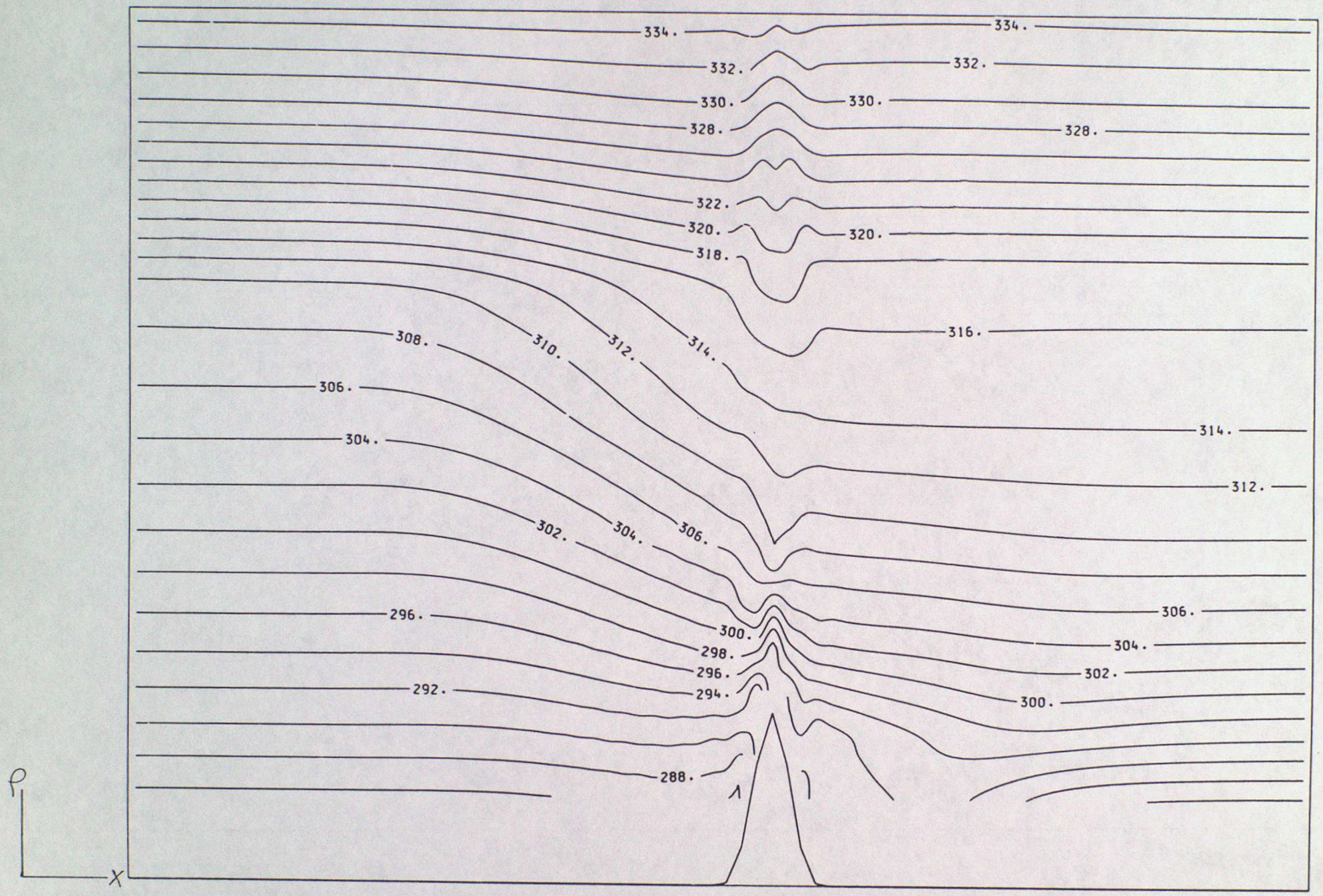
334.
334.
332.
332.
330.
330.
328.
328.
322.
320.
320.
318.
316.
308.
310.
312.
314.
306.
314.
304.
312.
302.
304.
306.
306.
304.
296.
300.
298.
302.
296.
294.
300.
292.
288.
P
X

Fig. 9b

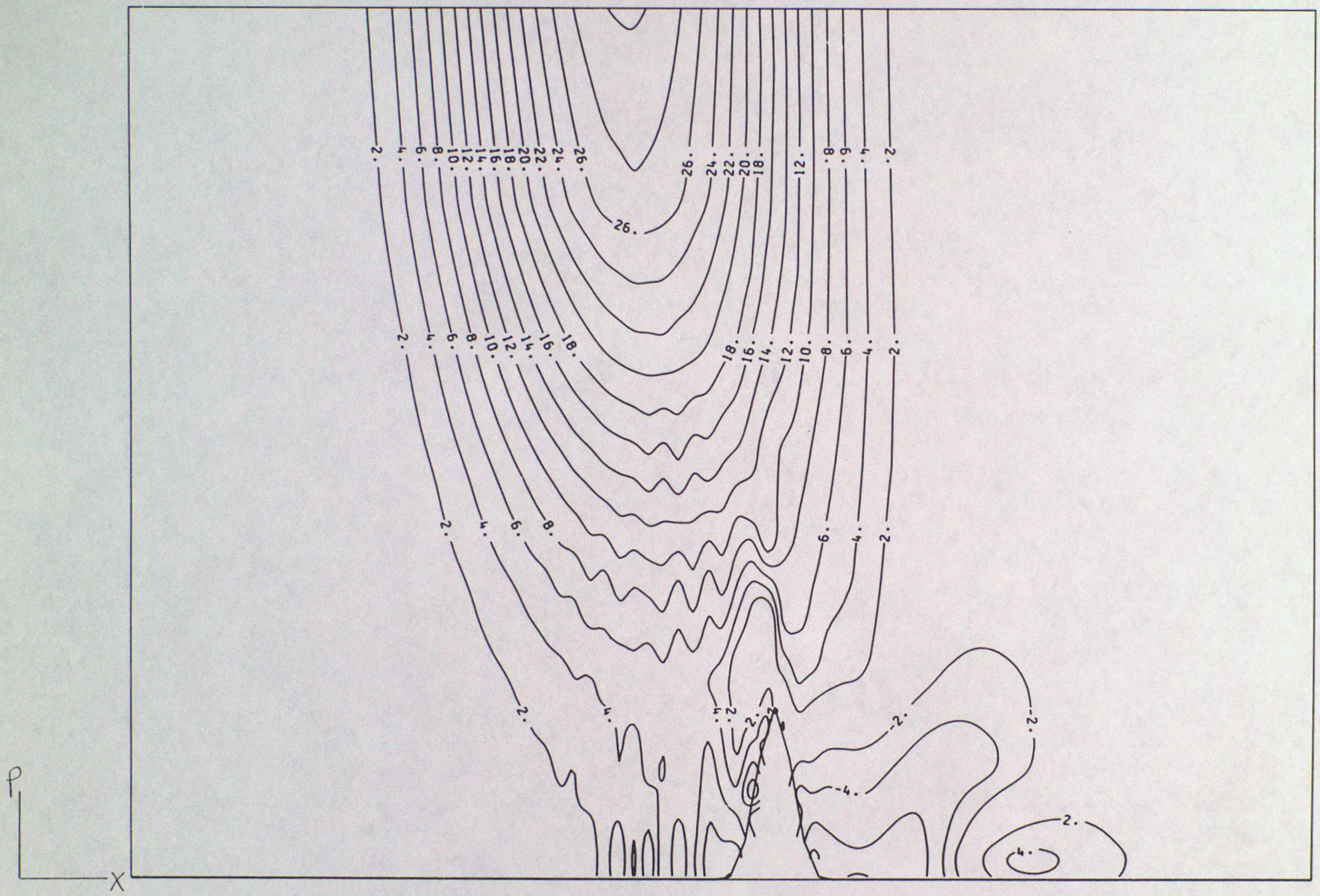

Fig.9c

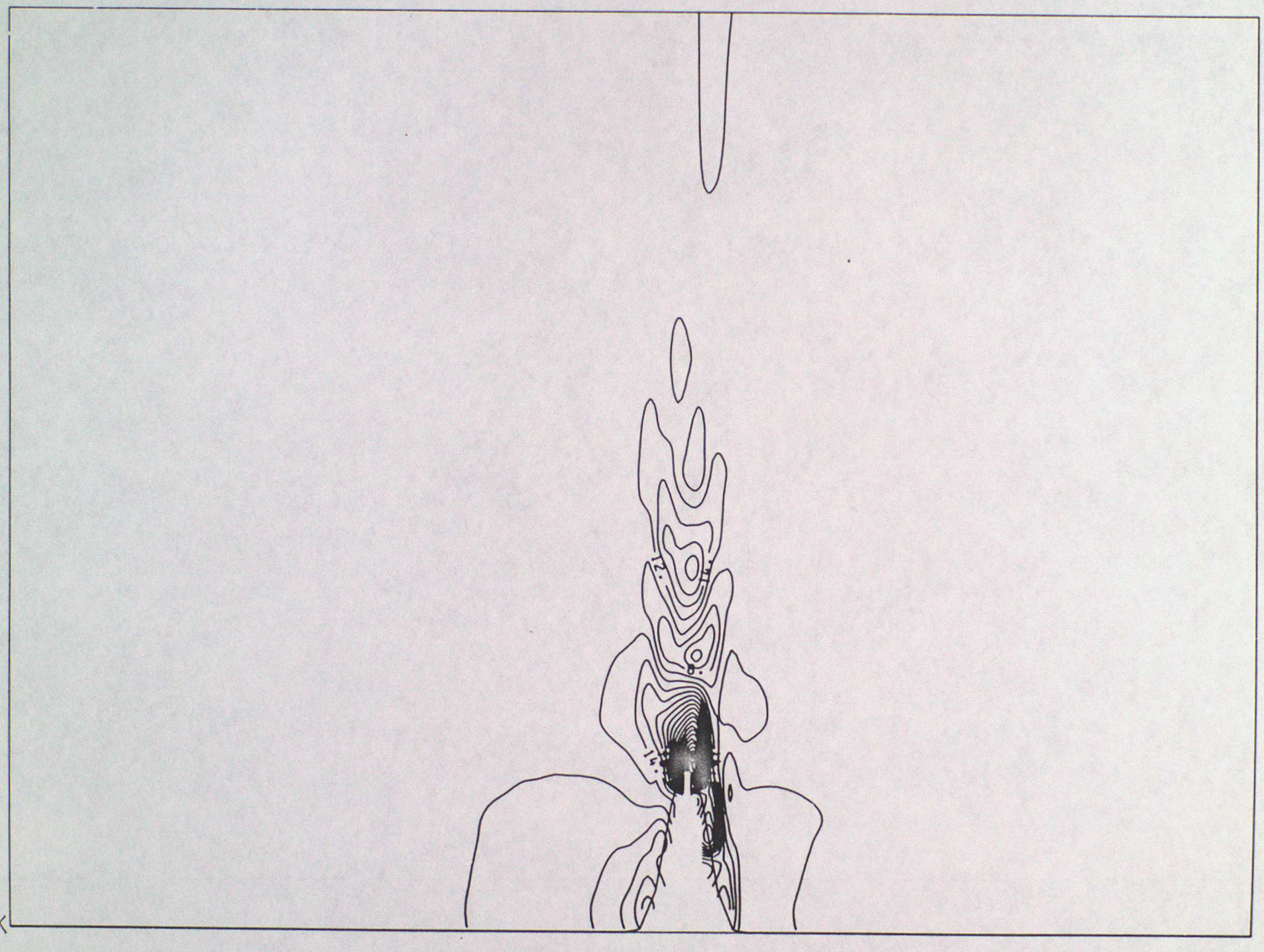

Fig. 9d

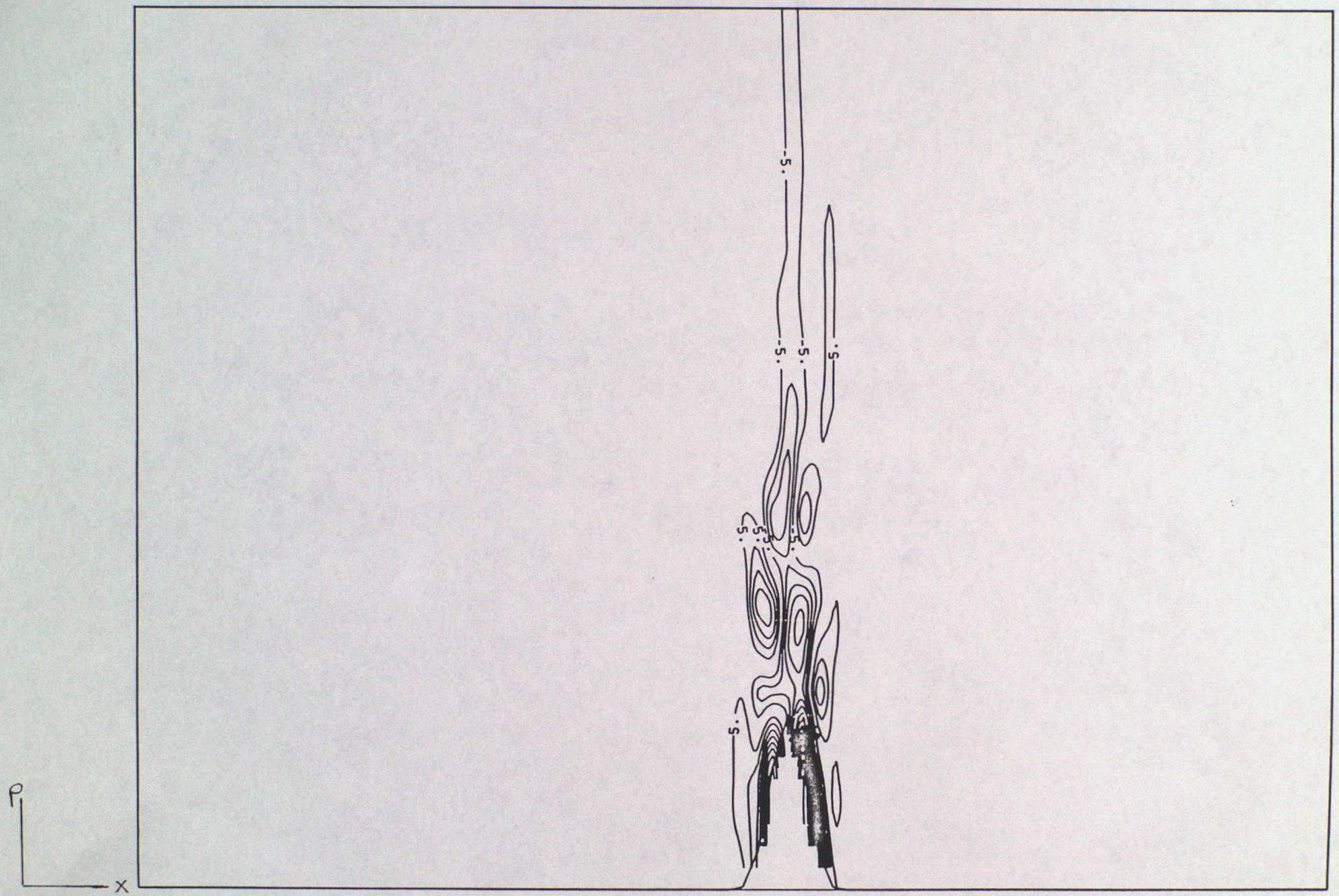

Fig. 9e